

The Global Content, Distribution, and Kinematics of Interstellar O VI in the Large Magellanic Cloud

J. Christopher Howk¹, Kenneth R. Sembach^{1,2}, Blair D. Savage³, Derck Massa⁴, Scott D. Friedman¹, & Alex W. Fullerton^{1,5}

ABSTRACT

We present *Far Ultraviolet Spectroscopic Explorer (FUSE)* observations of interstellar O VI absorption towards 12 early-type stars in the Large Magellanic Cloud (LMC). The observations have a velocity resolution of $\lesssim 20 \text{ km s}^{-1}$ (FWHM) and clearly show O VI 1031.926 Å absorption at LMC velocities towards all 12 stars. From these observations we derive column densities of interstellar O VI in this nearby galaxy; the observed columns are in the range $\log N(\text{O VI}) = 13.9$ to 14.6, with a mean of 14.37 and a standard deviation of $\pm 38\%$ ($^{+0.14}_{-0.21}$ dex). The observations probe several sight lines projected onto known superbubbles in the LMC, but these show relatively little (if any) enhancement in O VI column density compared to sight lines towards relatively quiescent regions of the LMC. The observed LMC O VI absorption is broad, with Gaussian dispersions $\sigma \approx 30$ to 50 km s^{-1} . This implies temperatures $T \lesssim (2 - 5) \times 10^6 \text{ K}$, indicating that much of the broadening is non-thermal because O VI has a very low abundance at such high temperatures. The O VI absorption is typically displaced $\sim -30 \text{ km s}^{-1}$ from the corresponding low-ionization absorption associated with the bulk of the LMC gas.

The general properties of the LMC O VI absorption are very similar to those of the Milky Way halo. The average column density of O VI and the dispersion of the individual measurements about the mean are identical to those measured for the halo of the Milky Way, even though the metallicity of the LMC is a factor of ~ 2.5 lower than the Milky Way. The velocity dispersion measured for the LMC material is also consistent with recent measurements of the Galactic halo. The striking similarities in these quantities suggest that much of the LMC O VI may arise in a vertically-extended distribution similar to the Galactic halo. We discuss the measurements in the context of a halo composed of radiatively cooling hot gas and/or turbulent mixing layers. If the observed O VI absorption is tracing a radiatively cooling galactic fountain flow, the mass flow rate from one side of the LMC disk is of the order $\dot{M} \sim 1 \text{ M}_{\odot} \text{ yr}^{-1}$, with a mass flux per unit area of the disk $\dot{M}/\Omega \sim 2 \times 10^{-2} \text{ M}_{\odot} \text{ yr}^{-1} \text{ kpc}^{-2}$.

Subject headings: galaxies: ISM – ISM: atoms – Magellanic Clouds – ultraviolet: ISM

¹Department of Physics and Astronomy, The Johns Hopkins University, Baltimore, MD, 21218; howk@pha.jhu.edu, scott@pha.jhu.edu, awf@pha.jhu.edu

²Current address: Space Telescope Science Institute, 3700 San Martin Dr., Baltimore, MD 21218; sembach@stsci.edu

³Astronomy Department, University of Wisconsin-Madison, Madison, WI, 53711; savage@astro.wisc.edu

⁴Emergent Information Technologies, Code 681, NASA's GSFC, Greenbelt, MD 20771; derck.massa@gsfc.nasa.gov

⁵Department of Physics and Astronomy, University of Victoria, P.O. Box 3055, Victoria, BC V8W 3P6, Canada

1. Introduction

Current theory suggests that the interstellar medium (ISM) in galaxies is strongly influenced by the input of energy and matter from stars. This is particularly true for spiral and irregular galaxies which are typically experiencing on-going star formation. The effects of the interactions of (multiple) stars and supernovae with the ISM in spiral and irregular galaxies is expected to produce pockets of super-heated gas (e.g., Heiles 1990; Norman & Ikeuchi 1989; Mac Low & McCray 1988), and the holes visible in the neutral hydrogen distributions of galaxies are often interpreted as the signature of such effects (Kim et al. 1999; Puche et al. 1992; Deul & den Hartog 1990; Brinks & Bajaja 1986). In regions with high densities of early-type stars, the energy input from the stars and supernovae can shape interstellar matter on kiloparsec scales. For disk galaxies, with larger pressure gradients in the vertical, z , direction than the radial direction, the super-heated, high pressure gas is thought to flow away from the disk, feeding matter and energy into the thick disk or halo of the system (e.g., de Avillez 2000; Norman & Ikeuchi 1989; Bregman 1980).

The Large Magellanic Cloud (LMC) is the nearest disk galaxy to the Milky Way. Its proximity ($d \sim 50$ kpc) and low inclination angle ($i \approx 30^\circ - 40^\circ$) provide a relatively clear view of this system (see Westerlund 1997), with very little foreground or line-of-sight confusion. The LMC has long served as a laboratory for studies of the ISM. Excellent maps of the ISM within the LMC are available for the warm ($\lesssim 10^4$ K) gas, both neutral (Kim et al. 1998) and ionized (e.g., Smith 1999; Kennicutt et al. 1995; Davies, Elliott, & Meaburn 1976), as well as the hot gas (Snowden & Petre 1994; Wang et al. 1991). The ability to resolve individual stars from each other and the ISM in this system provides a unique opportunity to determine the energy budget of the largest interstellar structures within the galaxy (e.g., Oey 1996).

Studies of the hot gaseous content of the LMC are of particular importance for understanding the energy input into the ISM from stars. One manner in which to study the hot gas content of a galaxy is through ultraviolet (UV) absorption line observations of the Li-like oxygen ion (O^{+5} or O VI), which has a doublet of transitions at 1031.926 and 1037.617 Å. The O VI ion principally arises in hot, collisionally-ionized gas in galactic environments since the ionization potential for its production ($IP_{O\text{V}-O\text{VI}} = 114$ eV) is high enough to preclude a significant photoionized component. Such observations are currently plausible using the *Far Ultraviolet Spectroscopic Explorer (FUSE)*, a dedicated spectroscopic observatory operating in the wavelength range 905 – 1187 Å at high resolution ($R \equiv \lambda/\Delta\lambda \approx 15,000 - 20,000$). *FUSE* can easily observe stars in the Galactic halo, stars in the Magellanic Clouds, and distant extragalactic sources with sufficient signal to noise to produce reliable O VI column density and line profile measurements.

Here we present *FUSE* spectra of O VI absorption towards 12 early-type stars in the LMC, the properties of which are summarized in Table 1. In this work we show that the LMC contains a large amount of highly-ionized gas distributed in a patchy manner across its face. The O VI column densities in the LMC along the directions studied in this work are as high as those observed through the halo of the Milky Way (Savage et al. 2000). We show that the hot material traced through O VI is present at significantly different velocities than the bulk of the low-ionization material arising in the disk of the LMC, a phenomenon that was also seen in *Hubble Space Telescope (HST)* observations of C IV absorption (Wakker et al. 1998). We will argue that the available evidence suggests much of the observed LMC absorption arises in an extended halo or corona, perhaps very similar to that observed in the Milky Way. These results are important since the LMC is the only other disk galaxy beyond the Milky Way that can be studied in this manner.

In §2 we discuss the reduction of the *FUSE* data employed in this work, while §3 discusses the methods used in analyzing the data. We discuss the gross distribution of O VI column densities in the LMC in §4, and the rough kinematic properties of the hot material in §5. In §6 we discuss the implications of our

observations, and we summarize our work in §7.

2. *FUSE* Observations and Data Reduction

The *FUSE* mission, its planning and in-orbit performance are discussed by Moos et al. (2000) and Sahnou et al. (2000). Briefly, the *FUSE* observatory consists of four co-aligned prime-focus telescopes and Rowland-circle spectrographs feeding two microchannel plate (MCP) detectors with helical double delay line anodes. Two of the telescope/spectrograph channels have SiC coatings providing reflectivity over the range $\sim 905 - 1105 \text{ \AA}$, while the other two have Al:LiF coatings for sensitivity in the $\sim 1000 - 1187 \text{ \AA}$ range. We make use of only the latter, the LiF channels, in this work. Light from each mirror passes through an aperture onto a holographically-ruled spherical grating. The resulting spectra are projected onto the MCP detectors, with spectra from one LiF and one SiC channel imaged in parallel onto each detector.

The data used in this work were all obtained with the source centered in the $30'' \times 30''$ (LWRS) aperture of the LiF1 spectrograph channel.⁶ In many cases, the LiF2 channel was co-aligned well enough with the LiF1 channel that a second set of spectra covering the 1000–1187 \AA wavelength range was obtained. Total exposure times ranged from 3.6 ksec to 33 ksec for the LMC stars used in this work. A log of the observations used for this investigation is given in Table 2.

The raw datasets consist of tables of time-tagged photon event locations within each 16384×1024 detector array.⁷ The individual exposures for a set of observations were merged into a single spectrum by concatenating the individual photon event lists. These combined time-tagged photon event lists were processed with version 1.8.6 or 1.8.7 of the standard *FUSE* calibration pipeline (CALFUSE) available at The Johns Hopkins University [see Oegerle et al. (2000) for a detailed description of the CALFUSE pipeline]. The differences between these two versions of the pipeline are inconsequential for our purposes. The photon lists were screened for valid data with constraints imposed for earth limb angle avoidance and passage through the South Atlantic Anomaly. Corrections for detector backgrounds, Doppler shifts caused by spacecraft orbital motions, and geometrical distortions were applied (Sahnou et al. 2000). No corrections were made for optical astigmatism aberrations, and no flatfield corrections are yet applied in the *FUSE* calibration process. Given the existence of significant fixed-pattern noise structure introduced by the *FUSE* detectors, the latter omission can be particularly important. We compared the LiF1 and LiF2 spectra whenever possible to determine the significance of the observed features.

The processed data have a nominal spectral resolution of $\lesssim 20 \text{ km s}^{-1}$ (FWHM), with a relative wavelength dispersion solution accuracy of $\sim 6 \text{ km s}^{-1}$ (1σ). The zero point of the wavelength scale for each individual observation is poorly determined. In a few cases *International Ultraviolet Explorer* (*IUE*) or Space Telescope Imaging Spectrograph (*STIS*) data allowed us to constrain the velocity zero point of observations of LMC stars. These include the sight line toward Sk-71° 45 with *STIS* and Sk-67° 211 with *IUE*. We have also investigated the velocity offsets of several stars not presented in this work and find that a consistent shift of ≈ -45 to -50 km s^{-1} from the CALFUSE wavelength solution was often appropriate to bring the *FUSE*

⁶The Sk-67° 05 data were obtained as part of in-orbit checkout activities that required multiple exposures with the object at different locations within the aperture. The processing of this observation required special care to ensure that the individual exposures were shifted and summed properly. The analysis of this sight line is discussed by Friedman et al. (2000).

⁷Bright targets make use of the spectral image mode wherein the photons arriving at each pixel are simply summed and read out at the end of the exposure. This mode does not preserve the time-tagged nature of the data.

data into the LSR frame (with the exception of the Sk-67° 05 datasets; see Friedman et al. 2000). This is consistent with the average shift of $-47 \pm 5 \text{ km s}^{-1}$ derived for *FUSE* LMC/SMC observations calibrated with STIS echelle-mode observations by Danforth et al. (2002). We note that this shift includes an implicit correction for the sign error in the application of the heliocentric velocity correction in all *CALFUSE* versions prior to v2.0, though the magnitude of this error is small for LMC sight lines (of order $\sim 5 \text{ km s}^{-1}$). In those cases where other data are not available, we have adopted a -50 km s^{-1} shift to the *FUSE* velocity scale.

Figure 1 shows portions of the final *FUSE* spectra of two stars near the O VI doublet: Sk-67° 211 and Sk-71° 45. These spectra represent only data from the LiF1 channel for each star. Several prominent ionic absorption lines are marked, with ticks showing the location of the Milky Way and LMC absorption components. The positions of the Milky Way and LMC ticks are determined by the velocity of the Si II line at 1020.699 Å. We have not marked the position of interstellar Ly β absorption. Telluric emission lines from Ly β and O I can be seen to varying degrees in the data.

These two sight lines represent two extremes of molecular hydrogen absorption for our sample of stars. The sight line towards Sk-71° 45 shows a rich spectrum of H₂ absorption from both Milky Way and LMC gas. The expected positions of the H₂ lines (for $\lambda \gtrsim 1018 \text{ Å}$ and $J \leq 4$ only) in both the Galaxy and LMC towards Sk-71° 45 are marked under the spectrum of that star. The sight line towards Sk-67° 211, however, shows only very weak H₂ absorption (e.g., the Lyman (5-0) R(3) transition at 1041.16 Å). We discuss the importance of H₂ contamination of the interstellar O VI profiles in §3.2. The properties of the H₂ absorption within the LMC are discussed by Tumlinson et al. (2001).

It should be noted from Figure 1 that the absorption from the weaker O VI transition at 1037.617 Å is almost always heavily confused by absorption from C II* and H₂ when studying the LMC. This is the case even for Sk-67° 211, which exhibits only very weak H₂ absorption.

3. Analysis of Interstellar O VI Absorption

This section discusses the details of our analysis of the interstellar O VI absorption. Of particular importance is the estimation of the stellar continuum, which is determined by the specifics of the out-flowing stellar wind for the stars in the sample (see §3.1). The estimation of the strength of H₂ contamination at the velocities of the interstellar O VI is more important for absorption at Milky Way velocities than for absorption at the velocities of the LMC, but in some cases it can be important for the latter as well (§3.2). Finally we discuss the details of our measurements of equivalent widths and column densities (§3.3).

3.1. Estimation of the Stellar Continuum

The single greatest uncertainty in an analysis of the interstellar O VI absorption from the LMC is the determination of the stellar continuum in the regions immediately surrounding the interstellar features. As discussed by Massa et al. (2002), the shape of the local stellar continuum in the O VI spectral region of early-type stars is dominated by resonance absorption (and scattering) of the stellar continuum emission by O VI ions in the out-flowing stellar wind. The principle source of O VI within the stellar winds of the O stars is likely ionization by X-rays produced in strong shocks propagating through the wind (Puls, Owocki, & Fullerton 1993). The radiative transfer of photons from the photosphere through the expanding wind yields a characteristic P Cygni-like profile (see Lamers & Cassinelli 1999). Because of the stochastic nature of the

shock formation process, the shape of the O VI P Cygni profiles can be significantly different for individual OB and WR stars and can even be temporally variable (e.g., Lehner et al. 2001).

Our approach to studying the interstellar O VI in this first study of the LMC is to use only stars whose stellar continua are straightforward to approximate. Furthermore, we have compared our fits of the stellar continua with the Sobolev Exact Integration (SEI; see Massa, Prinja, & Fullerton 1995) modelling of the radiative transfer of photospheric photons through the out-flowing stellar wind from Massa et al. (2002). We have insured that there are no significant systematic inconsistencies between the the stellar continua determined when viewing the stellar wind on a relatively local scale (i.e., within a few hundred km s⁻¹ of the ISM absorption) and the information derived from self-consistent radiative transfer models of the entire stellar wind profiles (with the provisos discussed by Massa et al. 2002).

We have limited our sample to WR stars and O stars with spectral types O7 and earlier. The use of only the earliest spectral types implies that we are using stars with large mass loss rates (and often large terminal velocities as well), which tend to show more fully developed (i.e., simpler) O VI P Cygni profiles and are less susceptible to difficulties caused by wind variations (see discussion below). To this end we have examined the existing *FUSE* PI team spectra of all stars meeting these spectral class requirements. From this sample we have chosen to study 12 sight lines: 11 new sight lines and 1 (Sk-67° 05) studied by Friedman et al. (2000). The properties of these 12 stars are summarized in Table 1.

Figure 2 shows the adopted stellar continua for the O stars (left column) and WR stars (right column) studied in this work. For each star we estimated the shape and level of the local stellar continuum near the interstellar O VI λ 1031.926 absorption by fitting low-order (≤ 5) Legendre polynomials to adjacent spectral regions free from interstellar lines. This fitting followed the techniques described by Sembach & Savage (1992), including the estimation of the uncertainties in the Legendre polynomial fitting coefficients. This allows us to include an estimate for continuum fitting uncertainties in our equivalent width and column density measurement error estimates (see below). In each case we adopted the lowest-order polynomial that could reasonably approximate the stellar continuum. Though we applied an *F*-test to assess the significance of additional polynomial terms, the final decision on the order of the fit was subjective.

A few general comments regarding the placement of stellar continua for early-type stars are necessary. The separation of the two members of the O VI doublet is ~ 1650 km s⁻¹. Thus, for stars whose winds have terminal velocities, v_∞ , in excess of this velocity, the absorption from the red member of the doublet will overlap that of the blue member. From the standpoint of understanding the stellar continuum in the region of interstellar O VI, stars with stellar wind terminal velocities within a few hundred km s⁻¹ of the 1650 km s⁻¹ separation of the O VI doublet are often problematic. Given that the terminal velocity is often manifested as a relatively sharp gradient in the absorption strength of the wind profile, stars with such terminal velocities can have relatively complex stellar continua in the region of interest for interstellar studies.

For terminal velocities $1650 \lesssim v_\infty \lesssim 2000$ km s⁻¹ the absorption edge of the 1031.926 Å transition lies in the deep interstellar Lyman- β trough or the 1037 Å transition overlaps the 1031.926 Å rest velocity. In both of these cases, the overlap with other transitions can make it very difficult to obtain a reliable SEI fit because the models typically try to simultaneously fit both lines of the doublet. With the exception of Sk-67° 05, the terminal velocities for the O stars in Table 1 are in excess of these values. The terminal velocities for the WR stars are all outside of this range (though we did not make use of SEI modelling of these stars). Our exclusion of lower terminal velocity O stars is not because of the difficulty of the SEI modelling, but rather because stars with lower terminal velocities often display more complex continua in

the region of interstellar O VI absorption. However, studies of the ISM towards later spectral type stars will need to consider the difficulties in the SEI modelling when comparing such models to their data.

Another concern regarding the general shape of the stellar wind absorption in the region of the O VI ISM lines is the probable variability of the stellar wind O VI absorption profiles. Lehner et al. (2001) have discussed such variations and their effects on continuum placement for interstellar studies. Using multiple *FUSE* observations of the O VI spectral region in Galactic and LMC stars, these authors showed that, even in sparsely sampled time series of two to three spectra, a large fraction ($\gtrsim 60\%$) exhibited some spectral variability over the time periods probed (days to months). In general the variability in the O VI P Cygni profiles happened at velocities much higher than those of the interstellar absorption towards these stars. Furthermore, the scale over which the O VI varies was typically several hundred km s^{-1} , significantly broader than most of the interstellar absorption lines in the Galaxy. Lehner et al. (2001) found that even though the shape of the stellar continuum can vary significantly with time, the derived O VI column densities and equivalent widths for Galactic absorption were typically not significantly different.

The situation for absorption in the LMC is less encouraging. Because the full extent of the absorption from the Galactic halo and the LMC typically extends over $\sim 300 - 400 \text{ km s}^{-1}$, the expectation that changes in the P Cygni profiles should occur over scales larger than that of the ISM absorption profile is no longer valid. Because the Milky Way absorption in these directions occurs at velocities of a few hundred km s^{-1} with respect to the rest frame of the stars, it is also no longer the case that most of the variation should occur at velocities well beyond the interstellar absorption. Indeed, the column densities and equivalent widths estimated towards the one LMC star in the study by Lehner et al. were significantly different between the two times sampled.

At this point we are unable to quantitatively assess the affects of stellar wind variability on the column densities derived along the sight lines to the LMC stars discussed in this work (see below). We note, however, that our choice of the earliest spectral type stars may help in this regard. Hot stars with large mass loss rates are desirable as background probes since their O VI wind lines are usually saturated. Nearly all of the flux observed in a saturated wind line is due to scattered light from throughout the wind. Therefore, substantial changes in the line of sight wind optical depth cannot have much of an impact on the flux profile because the transmitted flux is a small fraction of the total flux. The stellar wind profiles of these stars are therefore less susceptible to variations. The LMC star studied by Lehner et al. (2001) has a significantly lower terminal velocity and is of a later spectral type than the stars studied in this work. The continuum placement for this star is much more difficult than for any star in the present sample. This is important insofar as the column densities and equivalent widths of interstellar O VI can be accurately determined along the sight line to that star, irrespective of whether or not any variation in the wind profile is present.

Given the above discussion of wind variability and its effects on the derivation of O VI column densities, the reader should bear in mind that the column densities reported in this work have not been corrected for any stellar wind absorption features that may reside at velocities similar to the ISM features. Future re-observations of some of these stars are planned and may reveal some such features. However, the presence of discrete stellar wind absorption features at interstellar velocities can never be ruled out since one can only identify their presence if they change.

We should also note that for this work we have chosen to consider targets having relatively unambiguous separation between the stellar and interstellar features and well-delineated stellar continua, with the exception of Sk-67° 05. The continuum placement and uncertainties for this star, which also falls outside the range of spectral types we have investigated, are discussed in detail by Friedman et al. (2000). In general the

stellar continua are more complicated as one looks to later spectral types because the O VI P Cygni profiles of later type stars tend to be less well developed than those of the early O stars. As our understanding of the stellar winds of the later spectral-type stars improves, we may be able to make use of the larger sample of *FUSE* observations of late O and B stars in the LMC for studying interstellar O VI.

3.2. Assessing the Contamination from Molecular Hydrogen

Absorption from molecular hydrogen in both the Milky Way and the LMC can overlap the O VI absorption along the observed sight lines. Absorption from the (6-0) P(3) and R(4) transitions of H₂ at 1031.19 and 1032.35 Å, respectively, can contaminate the O VI absorption from the Milky Way halo and in some cases the O VI absorption from the LMC (e.g., see Figure 1). These lines absorb at -214 and $+123$ km s⁻¹ relative to the rest frame of O VI λ 1031.926. Rather than derive the detailed characteristics of the entire H₂ absorption spectrum, we have taken a more pragmatic approach to estimating the contamination of the interstellar O VI profiles by molecular hydrogen.

To estimate the contribution to the O VI profiles from the (6-0) P(3) and R(4) lines of molecular hydrogen, we have fit Gaussian profiles to a number of $J = 3$ and 4 transitions of H₂ with line strengths, $\log \lambda f$, very similar to the contaminating 6-0 band transitions. The H₂ transitions used in this approach are given in Table 3. For comparison, the properties of the contaminating (6-0) P(3) and R(4) lines are also given (in bold). We have only used lines which appear in the LiF1 channel. This helps to minimize the effects of changes in the breadth and shape of the instrumental line spread function, which occur when comparing lines in different channels and detector segments. Because of blending with other species and varying line strengths, the transitions available from Table 3 varied for each sight line.

The fitting process yields a peak apparent optical depth, a breadth, and a central velocity for each of the transitions. We have scaled the peak apparent optical depth for each fitted transition by the λf ratio of the contaminating 6-0 band line to that of the line fitted. Typically we were able to measure several transitions and average the scaled peak optical depths, breadths, and velocities predicted for the contamination (6-0) P(3) and R(4) transitions. For the $J = 3$ transitions we often measured both weaker and stronger transitions than the offending line. Where possible, we have fine-tuned the velocities using the Milky Way P(3) and LMC R(4) components on either side of the interstellar O VI profiles. A difficulty with this general approach is that saturation effects can be significant for unresolved spectral lines. We have attempted to circumvent such difficulties by judiciously choosing comparison transitions with line strengths λf close enough to those 6-0 band transitions that the factor by which the peak optical depths are scaled is small. In general we have found that the scaled peak optical depths for the comparison transitions show a smaller dispersion than the directly measured values.

Figure 3 shows the continuum-normalized interstellar absorption profiles of O VI towards all of the target stars listed in Table 2. The top panel shows the profiles with the model H₂ absorption spectrum over-plotted; the bottom panel shows the continuum-normalized profiles with the H₂ model divided out. The models include the Milky Way P(3) and LMC R(4) components, which were estimated using the same approach as the contaminating LMC P(3) and Milky Way R(4) absorption. Though these outlying components do not overlap the O VI absorption in which we are interested, they demonstrate the quality of our procedure for estimating the H₂ absorption strength.

For most of the sight lines studied in this work, the contamination of the O VI profile by molecular hydrogen absorption does not significantly affect the LMC absorption component. Notable exceptions include

the sight lines towards Sk–68° 80, Sk–71° 45, and to lesser extents Sk–67° 20, and Sk–69° 191.

The (6-0) R(0) transition of the HD molecule at 1031.912 Å is almost coincident with the rest wavelength of the strong O VI transition. For the sight lines towards the LMC stars studied here, contamination of O VI by this line is unimportant because the H₂ column densities, which are expected to be $\sim 10^4$ to 10^5 times stronger, are low (see Tumlinson et al. 2001). Furthermore, several HD lines of similar strength to the 6-0 band transition exist in the *FUSE* bandpass (see Sembach 1999) but are not seen in the spectra. We have, therefore, made no correction for HD contamination of the O VI absorption.

3.3. Interstellar Absorption Line Measurements

We measured equivalent widths and column densities of the interstellar O VI λ 1031.926 following Sembach & Savage (1992). We estimated interstellar column densities using the apparent optical depth method (Savage & Sembach 1991). The apparent optical depth, $\tau_a(v)$, is an instrumentally-blurred version of the true optical depth of an absorption line, given by

$$\tau_a(v) = -\ln [I(v)/I_c(v)] \quad (1)$$

where $I_c(v)$ is the estimated continuum intensity and $I(v)$ is the observed intensity of the line as a function of velocity. This is related to the apparent column density per unit velocity, $N_a(v)$ [atoms cm⁻² (km s⁻¹)⁻¹], by

$$N_a(v) = \frac{m_e c}{\pi e^2} \frac{\tau_a(v)}{f \lambda} = 3.768 \times 10^{14} \frac{\tau_a(v)}{f \lambda(\text{\AA})}, \quad (2)$$

where λ is the wavelength in Å, and f is the atomic oscillator strength. In the absence of *unresolved* saturated structure the $N_a(v)$ profile of a line is a valid, instrumentally-blurred representation of the true column density distribution as a function of velocity, $N(v)$. In the case of interstellar O VI absorption, the absorption profiles are typically broad enough to be fully-resolved by the *FUSE* spectrographs (e.g., see Savage et al. 2000). In the few cases where the weaker O VI 1037.617 Å line is clean enough to allow a comparison with the stronger line, no evidence for unresolved saturation has been found.

Table 4 lists the derived O VI the equivalent widths and column densities for the LMC material. The error estimates in Table 4 include contributions from statistical (photon) uncertainties and uncertainties in the continuum polynomial coefficients (see Sembach & Savage 1992). The effects of a 2% flux zero-level uncertainty are ~ 0.01 dex.

Also given in Table 4 is the range of velocities over which the absorption profile was integrated to yield the measurements given for the LMC material. The separation between Milky Way and LMC absorption is not always clearly demarcated in the spectra (see Figure 3). The separation is quite clear for the sight lines towards Sk–67° 05, Sk–67° 69, Sk–66° 100, Sk–67° 211, and Sk–66° 172. For the remaining sight lines, the derived properties of the LMC O VI absorption are somewhat dependent on the limits of the velocity integration. For the cases where the separation between the Milky Way and LMC absorption is not clear, we have adopted a standard lower velocity of $v = +175$ km s⁻¹, which is roughly typical of the sight lines for which the separation is relatively clear. For all of our measurements of the LMC O VI column densities, we have also derived these column densities at velocities ± 20 km s⁻¹ from the assumed lower velocity limit. The difference between the columns derived with these limits and that derived using the limits quoted in Table 4 is then treated as a 1σ uncertainty and added in quadrature to the statistical and continuum placement uncertainties discussed above. The estimated uncertainties derived using these ± 20 km s⁻¹ integration limits were in the range 0.02 to 0.09 dex ($\approx 5\%$ to 23%), with an average of ~ 0.05 dex ($\sim 12\%$).

4. Content and Distribution of O VI within the LMC

In this section we discuss the total column densities and distribution of interstellar O VI within the LMC. The stars in this work were chosen to have early spectral types and well-behaved O VI P Cygni profiles. Many of the stars in the sample were observed in order to study their stellar properties. As such we have not selected these sight lines based solely upon the properties of the LMC ISM in these directions. Even so, these sight lines probe a variety of physical regions within the LMC. We discuss the physical environments of the individual sight lines and compare the general distribution of O VI absorption with that of the gas traced by H α and X-ray emission.

4.1. Total Line-of-Sight O VI Column Densities

The integrated LMC O VI column densities span the range $\log N(\text{O VI}) \sim 13.9$ to 14.6 (in units of atoms cm^{-2}), i.e., a factor of ~ 5 . We have detected O VI absorption along all of the sight lines presented in this work. This is suggestive of a high surface covering factor of O VI in the LMC. We are hesitant to place too much emphasis on this result given that we have selected only early O and WR stars as background probes. The effects of the high wind luminosities of these stars on their local environments could in principle provide some of the observed O VI column densities. Figure 4 shows the column density of LMC O VI as a function of the spectral type of the background star. While there is no evidence for a dependence on spectral type, we sample a limited range of spectral types.

The statistics of the O VI column densities along the sight lines presented in this work are summarized in Table 5, including the straight and weighted means, standard deviation, and median of the sample. We give these statistics for the full sample of 12 stars shown in Table 4 and for the sample without the star Sk-67° 05. The sight line to this star was discussed by Friedman et al. (2000). Because of its late spectral type (O9.7 Ib) and relatively complex stellar continuum, we would not have included it in our sample had it not been discussed in detail previously. The medians and unweighted means of the two samples are very similar. We will henceforth discuss the values from the entire sample, with the caveat that one of our twelve sight lines may suffer from different systematic effects than the others.

As shown in Table 5, the average of the LMC column density measurements is $\log \langle N(\text{O VI}) \rangle = 14.37$ with a standard deviation of $\pm 38\%$ ($^{+0.14}_{-0.21}$ dex). The logarithm of the median of the measurements is 14.38. There is significant variation in the column densities between the individual sight lines. The separations of the background probes used here range from 0°5 to 5°1 (~ 450 to 4550 pc)⁸. Over the four smallest separations probed (450 to 510 pc), the absolute differences in the logarithmic column densities are 0.15, 0.17, 0.20, and 0.37 dex, corresponding to linear ratios of 1.41, 1.48, 1.58, and 2.34. The last value is for the Sk-67° 05/Sk-67° 20 pair, which we point out because of the potential uncertainties associated with the former star. We will discuss the distribution of O VI column densities more fully in §4.2.

An obvious point of comparison for interpreting the column densities of O VI in the LMC is the Milky Way. Savage et al. (2000) reported the first *FUSE* observations of interstellar O VI absorption in the disk and halo of the Milky Way as seen in the spectra of 11 active galactic nuclei (AGNs). These authors report a patchy distribution of O VI within the Milky Way halo. Defining the column density of O VI projected onto the plane of the Galaxy by $N_{\perp}(\text{O VI}) \equiv N(\text{O VI}) \sin |b|$, the sample of column densities in the Savage

⁸Throughout this work we adopt the canonical distance of 50 kpc to the LMC.

et al. (2000) sample has a mean $\log\langle N_{\perp}(\text{O VI}) \rangle = 14.29^{+0.14}_{-0.21}$ (std. dev.), with a median of 14.21 and a full range $\log N_{\perp}(\text{O VI}) = 13.80$ to 14.64 (a factor of ~ 7 range). In a plane-parallel exponentially-stratified layer the quantity N_{\perp} is simply the product of the midplane density, n_o , and the exponential scale height, h , of the distribution. Adopting a midplane density of $n_{\text{O VI}} = 2 \times 10^{-8} \text{ cm}^{-3}$ based on *Copernicus* observations (Jenkins 1978), Savage et al. find implied exponential scale heights in the range $h_{\text{O VI}} \approx 1.0$ to 7.0 kpc. Assuming an irregular distribution of absorbing clouds they derive a scale height for the clouds of $\sim 2.7 \pm 0.4$ kpc.

In order to compare the observed column densities in the LMC with those observed looking out from our position in the Galactic disk toward distant AGNs, it is useful to convert the LMC values to column densities projected perpendicular to the plane of the LMC, N_{\perp} , similar to the $N \sin |b|$ treatment of Savage et al. (2000). In the case of the LMC, that requires correcting the observed column densities for the inclination of the LMC. The inclination of the LMC is typically defined in terms of the angle of the disk plane from the plane of the sky, with values in the literature typically near $i \approx 33^{\circ}$ (e.g., Westerlund 1997). Hence, the correction factor is not the sine, but rather the cosine of the inclination from the plane of the sky. We find $\log\langle N_{\perp}(\text{O VI}) \rangle \equiv \log\langle N(\text{O VI}) \rangle \cos i = 14.29^{+0.14}_{-0.21}$ with the log of the median value being 14.30.

The average column density of O VI projected onto the plane of the LMC in our sample of 12 sight lines is identical to that projected onto the disk of the Milky Way, with the same degree of variation. We note that the same calculations excluding the sight line towards Sk-67° 05 yield an average column density higher by 0.03 dex (7%) with a lower standard deviation. We will discuss the implications of this comparison of the hot gas content of the Milky Way and LMC more fully in §6.

4.2. Comparison with Other Views of the LMC

The ISM of the LMC has been studied extensively over a range of wavebands. Given its proximity, these studies have provided a wealth of information on the warm ($\sim 10^4$ K) ionized gas traced through its $\text{H}\alpha$ emission and hot ($\gtrsim 10^6$ K) ionized material traced through its X-ray emission. Surveys of the former, in particular, have been used to identify large-scale structures in the ISM of the LMC that trace the feedback of energy from massive stars into the ISM (Henize 1956; Davies et al. 1976; etc.). $\text{H}\alpha$ imaging observations have revealed the presence of ionized structures on almost all scales, including H II regions, supernova remnants (SNRs), superbubbles, and “super-giant shells” (SGSs). The latter two classes of $\text{H}\alpha$ -emitting structures are the most prominent with projected diameters of ~ 100 to ~ 1000 pc.

4.2.1. Comparison with $\text{H}\alpha$ Distribution

Many of the stars in our *FUSE* sample are projected onto prominent $\text{H}\alpha$ -emitting structures. Table 6 lists the identification of any nebulosity and describes the general interstellar environments for each sight line. The identifications and descriptions rely heavily on previous studies. Examining Table 6 one can see a range of the general interstellar environments probed, including sight lines that are projected onto very faint $\text{H}\alpha$ emission associated with diffuse H II regions as well as objects that are projected onto prominent shells that have been identified as superbubbles. Several sight lines also probe the SGS LMC 4. Thus, while our sample of sight lines is small, it seems to probe a wide variety of physical regions.

Figure 5 presents a representation of the interstellar O VI column densities as a function of position on

the sky overlaid on an $H\alpha$ image of the LMC (Gaustad et al. 2001). The directions probed by our O VI measurements are marked with circles whose radii are linearly proportional to the integrated LMC O VI column densities along these lines of sight. Hence, Figure 5 shows a “map” of the O VI column density across the face of the LMC. A number is given next to each circle that denotes each sight line with the ID given in Table 4, and the circle in the upper right of the figure gives the scale for $N(\text{O VI}) = 10^{14} \text{ cm}^{-2}$. More detailed views of the $H\alpha$ -emitting gas projected near these sight lines can be found in Danforth et al. (2002).

Figure 5 gives an interesting view of the O VI distribution within the LMC. This figure demonstrates that relatively strong O VI absorption is present in regions where the ISM traced by $H\alpha$ is relatively quiescent. For example, the lines of sight to Sk-67° 20, Sk-66° 51, and Sk-67° 69 (numbers 2 through 4 in Figure 5) all probe regions of only relatively diffuse $H\alpha$ emission in quiescent regions of the galaxy (the bright spot near the last of these is due to an incompletely-subtracted foreground star), though their O VI column densities exceed 10^{14} cm^{-2} .

It can also be seen from Figure 5 that several stars (e.g., Sk-66° 100, Sk-67° 144, and Sk-66° 172 – numbers 7, 8, and 12) probe the periphery or interior of the SGS LMC 4, a 1400 pc diameter ring delineated by H II regions and encompassing an H I void (Kim et al. 1998) centered at $\alpha_{J2000} \approx 05^h 31^m 33^s$; $\delta_{J2000} \approx -66^\circ 40' 28''$. Furthermore, those lines of sight south of $\delta_{J2000} = -68^\circ$ are all projected onto previously-identified “supershells” in $H\alpha$ and X-ray studies (e.g., Dunne, Points, & Chu 2001). While two of these four sight lines exhibit the largest column densities in our sample (Sk-68° 80 and Sk-71° 45 – numbers 5 and 9, which probe N144 and N206, respectively), the other two have column densities consistent with the median of the sample.

The O VI column densities observed along our 12 sight lines seem to have little relation to the observed morphological structure of $H\alpha$ emission (Gaustad et al. 2002) in these directions. Furthermore, there is no relationship between the observed O VI column densities and the local star formation rate as traced by the intensity of the $H\alpha$ emission. Figure 6 shows the observed O VI column densities as a function of the relative $H\alpha$ intensity integrated over $6'.6 \times 6'.6$ ($100 \times 100 \text{ pc}^2$) regions surrounding the target stars. The range in $H\alpha$ surface brightness measurements is much larger than the range in O VI column densities.

The sight lines probing superbubbles and supergiant shells have O VI column densities quite similar to those projected onto more quiescent regions of the galaxy, and our derived O VI column densities have no observable relationship to the local $H\alpha$ intensity within the LMC. Thus, there is no evidence for large enhancements in the O VI column densities associated with large-scale structures or high levels of local star formation. As discussed in §6, this is consistent with a scenario in which much of the observed O VI resides in an extended, but patchy, distribution such as a galactic “corona.”

4.2.2. Comparison with X-ray Distribution

Hot ionized material in galaxies can also be revealed through observations of its X-ray emission. The general distribution of X-ray emission in the LMC has been studied with several instruments including the *Einstein Observatory* (Wang et al. 1991) and *ROSAT* (Snowden & Petre 1994). These studies have discussed the observations in the context of the diffuse, hot ISM in the LMC. Many studies detailing various aspects of individual regions of the LMC have also been published. The most relevant for comparison with this work are recent summaries of X-ray emission from superbubbles (Dunne et al. 2001) and large-scale diffuse regions, including SGSs (Points et al. 2001). These works include discussions of diffuse X-ray emission from

some of the structures (regions) probed by our absorption line measurements.

In general it is difficult to study the soft X-ray emission from the LMC given the relatively large foreground photoelectric opacity. Unfortunately, this is the waveband that is most likely to correspond to the material being traced by our O VI absorption line measurements. However, the harder X-ray emission traces gas at relatively high temperatures ($10^6 - 10^7$ K) which will presumably cool through the temperatures ($\lesssim 3 \times 10^5$ K) at which O VI is expected to be most abundant. Therefore, one might expect at least a loose connection between these two tracers of hot ionized matter. Figure 7 shows the *ROSAT* PSPC mosaic of the LMC from Snowden & Petre (1994) with the O VI columns from this work displayed as in Figure 5. The X-ray mosaic makes use of the R4 to R7 filters of the PSPC, which are sensitive to ~ 0.5 to 2.0 keV photons, and has been adaptively smoothed, as discussed in Snowden & Petre. This energy range is non-uniformly affected by photoelectric absorption by LMC and Milky Way gas. Point sources (e.g., X-ray binaries and background AGNs) have not been removed.

The main purpose of presenting this mosaic in comparison with our O VI measurements is to demonstrate that the sight lines probed in this work do not, in fact, probe regions of the LMC that are unusually X-ray bright. Our sample includes observations of a star projected onto the superbubble N144 and three sight lines projected onto the SGS LMC 4. Recent work on archival *ROSAT* PSPC data have shown that these regions do not have excessively high X-ray surface brightnesses (Dunne et al. 2001; Points et al. 2001). Indeed, supernova remnants are the largest contributors to the interstellar X-ray emission of the LMC, while superbubbles and SGSs are collectively more than a factor of two lower (Points et al. 2001). In general our sight lines do not probe regions where the amount of hot gas is atypically large for the LMC.

Figure 8 shows the observed O VI column densities compared with the relative X-ray surface brightness from *ROSAT* (Snowden & Petre 1994) for each sight line. The X-ray surface brightnesses were calculated for boxes $6'.6$ (100 pc) on a side, centered on the star of interest. No correction for overlying photoelectric opacity has been made in deriving the X-ray brightnesses. A linear relationship of slope unity between the two datasets is shown with the dashed line in the plot. We note that if the lowest point is left out (representing the sight line towards Sk-67° 05), this diagram becomes a scatter plot with no discernible relationship between the O VI column density and X-ray surface brightness measurements. Indeed, a Spearman’s rank-order correlation test (Press et al. 1992) cannot rule out the null hypothesis that the O VI columns and X-ray surface brightnesses are uncorrelated at the 2σ level. The significance of any correlation between the quantities is small. Given the very different way in which these measurements are made, the differing systematics to which they are subject, and the different gas traced by each approach, it would be surprising to find a significant correlation.

The four sight lines in our sample probing superbubbles are denoted with open circles in Figure 8, while the other sight lines are marked with filled circles. The superbubble sight lines have the highest four X-ray surface brightnesses, though their O VI column densities are not so easily separated from the other measurements. This may suggest that local effects are more important for determining the hard X-ray brightness than they are for determining the O VI column densities. However, the *ROSAT* “beam” is much larger than that probed by our absorption line measurements, and we do not know that the stars used as background probes do indeed lie behind the gas associated with the superbubbles.

5. Gross Kinematic Properties of O VI within the LMC

Figure 3 demonstrates two items of note regarding the kinematics of the observed O VI absorption: 1) There is a large degree of variation in the observed kinematic profiles of the Milky Way/LMC absorption complex; and 2) Separating the Milky Way and LMC components is non-trivial in some cases. The identification of O VI absorption in the velocity range $150 \lesssim v \lesssim 200 \text{ km s}^{-1}$ with either of the two galaxies is particularly difficult. At lower velocities, profiles such as those seen towards Sk-66° 100, Sk-67° 69, and Sk-67° 211 strongly suggest a Milky Way (including high- and intermediate-velocity cloud) origin. However, there is not easily-identifiable separation between Milky Way and LMC absorption in profiles such as those towards Sk-70° 91 and Sk-67° 20. This ambiguity between the absorption from the two galaxies makes it difficult to definitively discuss the kinematics of the absorption from the LMC. In particular, some of the material in this intermediate range could be caused by outflows from the LMC with velocities of $\sim 100 - 150 \text{ km s}^{-1}$. If this is the case, it is an important aspect of the LMC O VI kinematics, although one that cannot be addressed by the current observations.

Even in the presence of such ambiguities, there is useful information on the kinematics of the LMC O VI within the observed absorption profiles. We discuss two particular aspects of the LMC O VI kinematics in this section: a comparison of the O VI velocity profiles with those of the lower-ionization material traced by Fe II; and the kinematic properties of the O VI in directions where there is a clear separation between the Milky Way and LMC absorption.

Figure 9 shows a comparison of the O VI $\lambda 1031.926$ absorption line profiles (cleaned of H₂) with the Fe II $\lambda 1125.448$ profiles. The latter trace low-ionization gas associated with the relatively high column density warm neutral and warm ionized media in the Milky Way and LMC. Presumably most of the material in these cooler phases ($\sim 10^3 - 10^4 \text{ K}$ gas) resides in or near the disk of each galaxy. Examining the Fe II profiles, one can see clear signatures of Milky Way, intermediate- and high-velocity clouds (IVCs and HVCs), and LMC absorption. All of the sight lines in our sample show evidence for either IVC and/or HVC absorption. Though these components are not always readily visible in the Fe II $\lambda 1125.448$ profiles, the stronger Fe II 1144.938 Å and O I 1039.230 Å transitions show this to be the case (see the profiles presented in Danforth et al. 2002). The LMC often exhibits multiple components or complex absorbing structure. The stronger Fe II 1144.938 Å transition often shows much lower column density components that are not visible in the Fe II $\lambda 1125.448$ profiles.

The individual Fe II components are more easily separated than those in the O VI profiles because the widths of typical Fe II absorption complexes is significantly lower than those seen in O VI absorption. Good examples of this effect are seen in the spectra of Sk-67° 69, Sk-68° 80, and Sk-67° 211. The differences between the Fe II and O VI absorption could be caused by larger thermal broadening within the hot ISM traced by the O VI absorption. While this is in part the case, we show below that the individual O VI absorbing complexes are much broader than expected from pure thermal broadening.

The O VI profiles almost always extend to lower velocities than the Fe II absorption. Furthermore, in cases where the LMC O VI absorption is well separated from the Milky Way, it tends to be somewhat symmetric and centered at velocities well below those of the Fe II absorption complexes. The Fe II absorption is often aligned with the high-velocity edge of the O VI absorption. Thus the O VI often appears to be kinematically decoupled from the Fe II, which traces material predominantly associated with the disk of the LMC.

A similar effect, but opposite in sign, can be seen when comparing the O VI and Fe II absorption from

the Milky Way. The Fe II typically traces the low-velocity edge of the O VI absorption, the latter extending to much higher velocities. This may in part be caused by the stronger influence of the IVCs and HVCs on the O VI profile. However, because Galactic rotation Doppler shifts distant gas to positive velocities in this direction, much of this effect could also be caused by the larger vertical extent of O VI compared with Fe II.

Several sight lines show enough separation between the Milky Way and LMC O VI absorption that the detailed kinematic properties of the LMC absorption can be ascertained. We have fit Gaussian components to the apparent optical depth profiles for several lines of sight, deriving the average velocity, breadth, and peak optical depth for the LMC absorption seen towards these stars. We assume that the LMC absorption can be approximated by a single Gaussian component. In most cases this gives a reasonable approximation to the observed absorption profiles. In these cases we have also fit the Milky Way absorption to account for any minor blending with the LMC absorption. We do not report the Milky Way results here, particularly because there is a large degree of ambiguity when fitting the O VI profiles with multiple Gaussians.

The absorption profiles fit in this way include those towards the stars Sk–67° 69, Sk–66° 100, Sk–67° 211, and Sk–66° 172. Further decomposition of the profile towards Sk–71° 45 is discussed by Lauroesch et al. (2002). The most important aspect of these fits is the derived dispersion of the LMC O VI absorption. For the sight lines listed we derive $\sigma = 37, 30, 41,$ and 48 km s^{-1} , respectively. The corresponding FWHM (Γ) values are $\Gamma = 87, 71, 96,$ and 113 km s^{-1} . This range of widths implies temperatures for the absorbing regions $T \leq 2 \times 10^6$ to $\leq 5 \times 10^6 \text{ K}$. If the observed gas is closer to the temperature at which the abundance of O^{+5} peaks in collisional ionization equilibrium ($T \sim 3 \times 10^5 \text{ K}$), most of the observed breadths of these profiles must be caused by non-thermal broadening mechanisms, including turbulence, multiple velocity components, and large-scale dynamical effects. Given the smoothness of the profiles observed at high signal-to-noise ratios, it seems likely that if this breadth is due to multiple absorbing components along the line of sight then several such components may be required.

Savage et al. (2002) have measured the apparent breadths of the absorption from the O VI within the halo (or thick disk) of the Milky Way as seen towards a large number (~ 85) of extragalactic sources. These authors find $\sigma \approx 16$ to 65 km s^{-1} ($\Gamma \approx 37$ to 153 km s^{-1}) with a median of $\sigma \approx 39 \text{ km s}^{-1}$. The observed breadths towards lower latitude sources may be affected by Galactic rotation, although many of their sight lines are at high enough Galactic latitudes that such effects are unimportant. The median breadth from these large number of measurements through the Galactic halo is essentially equivalent to that of the four LMC measurements (median $\sigma = 39 \text{ km s}^{-1}$). For comparison, Jenkins (1978) has discussed the breadths of nearby ($d \lesssim 1000 \text{ pc}$) disk O VI absorption as observed by *Copernicus*; he found an average dispersion of $\sigma \approx 29 \text{ km s}^{-1}$.

We have also fit Gaussian profiles to the observed Fe II absorption for the four sight lines listed above to determine the central velocities of the LMC Fe II. Of interest in these cases is the relative difference between the average velocities of the O VI and Fe II absorption. For this small sample of sight lines, we find that an average velocity difference, $\Delta v \equiv v_{\text{O VI}} - v_{\text{Fe II}} = -32 \text{ km s}^{-1}$. The central velocity of the O VI is on average shifted by -32 km s^{-1} relative to central velocity of the Fe II along these lines of sight. Because the O VI is significantly broader than the Fe II, much of the O VI absorption occurs at velocities significantly lower than the bulk of the Fe II absorption (which can be seen in Figure 9). This average velocity separation may not be typical of all of the sight lines since we have examined only those directions that show a clear separation between the Milky Way and LMC O VI absorption.

We note that our observations cannot be used to test the existence of high-velocity outflows from the disk of the LMC. Material separated from the LMC disk velocity by $v - v_{\text{disk}} \lesssim -75 \text{ km s}^{-1}$ is confused with

Galactic ISM, IVC, and HVC absorption. In almost all of the sight lines there is O VI absorption at velocities shortward of the Fe II absorption associated with the LMC disk (but longward of the $\sim +150$ to $+175$ km s $^{-1}$ separation between LMC and HVC material). O VI absorption is usually not detected at positive velocities relative to the Fe II from the LMC disk. The two exceptions to this are Sk-68° 80 and perhaps Sk-70° 91. The Fe II profile towards the latter object shows several LMC components with similar strength, making the identification of the “disk” component somewhat ambiguous. Towards Sk-68° 80 O VI absorption extends to velocities $\sim +60$ km s $^{-1}$ higher than the Fe II 1125.448 Å absorption. A very weak component can be seen in the Fe II 1144.938 Å line at $v \sim +275$ km s $^{-1}$, though the bulk of the Fe II absorption in this direction is centered at $v \sim +240$ km s $^{-1}$. The extended high positive-velocity absorption seen in the O VI profile towards Sk-68° 80 may be evidence for infalling material along this sight line. However, at least 10 of the 12 sight lines studied in this work reveal no such absorption, suggesting infalling highly-ionized material is rare in the LMC.

6. Discussion: the Hot Corona of the LMC

Our observations of interstellar O VI associated with the LMC reveal that this tracer of hot, collisionally-ionized gas is present in relatively large quantities across the whole face of the LMC, though with a large degree of patchiness. Lines of sight projected onto superbubbles and supergiant shells have much the same column densities as lines of sight projected onto quiescent regions (as indicated by H α emission). The velocity distribution of the LMC O VI absorption is significantly different than that of lower-ionization gas (e.g., Fe II), being both much broader and present at lower absolute velocities.

The average column density projected onto the plane of the LMC (N_{\perp}) is equivalent to that projected onto the plane of the Milky Way, as determined by measurements of the Galactic halo towards extragalactic sources (Savage et al. 2000). The dispersion in the measurements of N_{\perp} in the LMC and Milky Way is also the same. The kinematics of the highly-ionized gas traced by O VI in the LMC seems to be very similar to that seen through the halo of the Milky Way, although our ability to accurately measure the kinematic profiles of the LMC absorption is limited.

There are several possible interpretations of these salient aspects of the LMC O VI absorption observed towards our sample of 12 stars. However, given the striking similarities between the properties of the LMC O VI and the Galactic halo O VI, the relatively small impact of superbubbles on the total O VI column densities, the existence of significant quantities of O VI along sight lines with little evidence for local sources of highly-ionized material, and the general decoupling of the O VI kinematics from the disk material traced by Fe II, we favor an interpretation in which the LMC O VI absorption arises in a vertically-extended halo or corona similar to that seen about the Milky Way (see Savage et al. 2000).

6.1. Alternative Interpretations

Before exploring the O VI corona interpretation in more detail, it is worth mentioning alternatives to this scenario. Sembach et al. (2000) have presented observations of O VI in the HVC system surrounding the Galaxy. Most (if not all) sight lines that pass through known H I HVCs show O VI absorption, including the Magellanic Stream (MS), material tidally-expelled from the LMC/SMC system. If the MS has a component projected between the Sun and the LMC, the observed O VI at LMC velocities (or at the IVC and HVC velocities) could be associated with this tidal structure. For this to be true, however, the ionization state of

the Stream in these direction would be significantly different than other directions probing this structure (and than most other HVCs). Given that the observed Fe II absorption can be associated with LMC disk material (see, e.g., Danforth & Chu 2000) and is typically centered well away from the center of the O VI absorption, relatively little low-ionization material could be associated with such a putative Stream component.

Another possibility is that the O VI absorption traces the interaction between the gaseous coronae of the LMC and Milky Way. The presence of O VI in the MS strongly suggests the Milky Way halo extends to the distance of that structure, which is roughly $\sim 25 - 75$ kpc from the Sun (see the discussion by Sembach et al. 2000). It is therefore reasonable to expect that the Galactic corona extends to the 50 kpc distance ($z \sim 25$ kpc) of the LMC. Interactions between the LMC corona (or other portions of this galaxy) with the low-density, highly-ionized medium associated with the extended distribution of hot gas of the Milky Way could, in principle, provide for instabilities that cool the gas through the transition temperatures at which O^{+5} is abundant. [de Boer et al. (1998) have similarly suggested that the motion of the LMC through the Galactic halo can trigger star formation through the compression of LMC material along the leading edge of the LMC by the low density Milky Way material.] Given the large number of unknowns regarding the structure of the ISM of the LMC and the extended Galactic halo, this model remains largely unconstrained. Unfortunately, at this point, it is difficult to falsify either of the previous models.

6.2. The Origins of O VI in the Corona of the LMC

The scenario we prefer is one in which the O VI within the LMC is distributed within the thin disk as well as in a more vertically-extended thick disk or halo of the LMC. Since our lines of sight probe large pathlengths through the halo component, this dominates over material associated with the disk, in a manner analogous to observations of extragalactic sources from within the disk of the Milky Way (Savage et al. 2000). The presence of a possible corona about the LMC has been discussed in the literature for several years. Early observations of C IV absorption towards LMC stars with the *IUE* observatory revealed highly-ionized material at velocities consistent with an LMC origin (Savage & de Boer 1979, 1981; de Boer, Koornneef, & Savage 1980; de Boer & Savage 1980). The early *IUE* measurements of LMC material were interpreted as absorption from an extended hot corona. That interpretation was subsequently called into question (Chu et al. 1994; Feitzinger & Schmidt-Kaler 1982) because of the strong possibility that the high ions observed were produced in the local environments of the observed stars. Wakker et al. (1998) used *HST* observations of C IV towards stars in quiescent regions of the LMC to argue that the LMC did indeed contain a highly-ionized corona. The data to date, however, have been too sparse to firmly detail the properties of the highly-ionized material in the LMC.

The O VI absorption in this coronal scenario traces material at relatively large distances from the disk that has been heated and ejected from the disk by some form of feedback between massive stars and the ISM. Most calculations suggest this requires the collective actions of multiple, correlated supernovae (particularly to raise the material far above the plane). There are several possible microphysical origins for the O VI within an extended corona about the LMC. Highly-ionized halo gas may trace material cooling from higher temperatures through the transition temperatures (a few $\times 10^5$ K) at which O VI is abundant or material created in the interactions between cooler (e.g., 10^4 K) and hotter (e.g., $> 10^6$ K) gases (e.g., in conductive interfaces or turbulent mixing layers). These two broad types of models have significantly different predictions for the O VI columns through a hot corona. As such, the interpretation of the observed O VI column density depends upon which microphysical situation is most applicable. We discuss the details of each of these models below.

6.2.1. Radiative Cooling Models

Edgar & Chevalier (1986) have calculated the column densities of highly-ionized species for gas cooling from temperatures $T \gtrsim 10^6$ K. They show that for cases where the cooling is dominated by metal line emission, the expected column density of O VI and the other high-ions is independent of metallicity. The expected column density of a metal ion, Z^i , in a column of cooling material is $N(Z^i) \propto A_Z \dot{N} t_{\text{cool}}$, where A_Z is the abundance of the element Z with respect to hydrogen, \dot{N} is the flux of cooling material (in ionized hydrogen atoms $\text{cm}^{-2} \text{s}^{-1}$), and t_{cool} is the cooling time. The cooling time is inversely proportional to the abundance of metals, making $N(Z^i)$ independent of A_Z . This is important for the LMC because the abundance of oxygen is $A_{\text{O}} \approx 2.2 \times 10^{-4}$ (Russell & Dopita 1992; see also Appendix of Welty et al. 1999), a factor of ~ 2.5 below the recently updated solar value of $A_{\text{O}} \approx 5.4 \times 10^{-4}$ (Holweger 2001).

Because $t_{\text{cool}} \propto n_{\text{H}^+}^{-1}$, where n_{H^+} is the initial ionized hydrogen density of the cooling material, the column density of highly-ionized metals in the radiatively-cooling flows discussed by Edgar & Chevalier (1986) is proportional to \dot{N}/n_{H^+} , which, by conservation of mass is simply a velocity, v . The Edgar & Chevalier calculations predict a column density of $N(\text{O VI}) \sim 4 \times 10^{14} (v/100 \text{ km s}^{-1})$. This value is sensitive to the peak temperature from which the gas cools, which is assumed to be 1×10^6 K. If the peak temperature is 3×10^6 K, the column density is increased by a factor of ~ 2 . Using the mean value of $N(\text{O VI})$ from Table 5, the expected velocity associated with an Edgar & Chevalier-like flow is in the range $v \sim 30$ to 60 km s^{-1} . The lower portion of this range (which corresponds to higher initial cooling temperatures) is crudely consistent with the observed velocity separation between the O VI and Fe II absorption.

Since models of radiatively cooling gas predict the column density of O VI to be independent of metallicity, they provide a natural explanation for the similarities between the values of N_{\perp} in the Milky Way and the LMC. For the Edgar & Chevalier models, so long as the ratio $v \equiv \dot{N}/n_{\text{H}^+}$ is similar in the two systems, the column densities of the observed O VI absorption should also be similar.

In the context of a cooling flow like that described by Edgar & Chevalier (1986), the column density of O VI is related to the mass flow rate out of the disk, \dot{M} :

$$\dot{M} \approx (\mu m_{\text{H}}) n_{\text{H}^+} \Omega \left(\frac{\dot{N}}{n_{\text{H}^+}} \right). \quad (3)$$

In this expression μm_{H} is the mean mass per atom, and Ω is the surface area of the flow region, which we take to be the disk of the LMC assuming a diameter of ~ 7.3 kpc, the diameter of the H I disk (Kim et al. 1998). For gas cooling under isobaric conditions from 1×10^6 K, Edgar & Chevalier find $\dot{N}/n_{\text{H}^+} \sim 2.5 \times 10^6 [N_{\perp}(\text{O VI})/10^{14} \text{ cm}^{-2}]$. These values yield an estimate for the mass-flow rate from the near side of the plane of the LMC:

$$\dot{M} \sim 1 \left(\frac{n_{\text{H}^+}}{10^{-2} \text{ cm}^{-3}} \right) M_{\odot} \text{ yr}^{-1}. \quad (4)$$

The initial density of the cooling gas, n_{H^+} , is an unknown. Points et al. (2001) estimate electron densities of the X-ray emitting gas in the range $n_e \gtrsim (0.3 - 2) \times 10^{-2} \text{ cm}^{-3}$ in their study of the X-ray emission from supergiant shells and diffuse gas in the LMC. Dunne et al. (2001) estimate electron densities of X-ray emitting gas in LMC superbubbles in the range $n_e \gtrsim (1 - 10) \times 10^{-2} \text{ cm}^{-3}$. These estimates depend upon the estimated volume occupied by the X-ray emitting material, and a filling factor of unity for the material is assumed (the predicted densities increase as the assumed filling factor decreases). The O VI column densities themselves can also be used to crudely estimate density limits for the hot ionized material. If we assume that the pathlength through LMC material probed by our observations is no greater than the 7.3 kpc diameter of the LMC assumed above, the average density of O VI ions is $\langle n_{\text{O VI}} \rangle \equiv N(\text{O VI})/d \gtrsim 10^{-8} \text{ cm}^{-3}$. This

corresponds to average ionized hydrogen densities of $\langle n_{\text{H}} \rangle \gtrsim 2 \times 10^{-4} \text{ cm}^{-3}$ assuming the fraction of oxygen in the form of O VI is at its maximum expected value of ~ 0.2 (Sutherland & Dopita 1992). The true density of ionized hydrogen in the O VI-bearing gas will likely be substantially larger since the fraction of space occupied by this material is likely to be small. We note, however, that the densities suggested by this crude treatment of the O VI column densities and the X-ray analyses (which are biased towards high density material that is more likely to be in the plane of the LMC) probably bound the physical ionized hydrogen density in the O VI-bearing gas.

The estimated mass-circulation rate from the LMC is a factor of ~ 10 lower than the values typically estimated for the Milky Way assuming the same initial densities. The main cause of this difference is the much different surface areas assumed for the disks of the two galaxies. The mass-flow rate per unit area of the disk for the LMC is

$$\dot{M} \sim 2 \times 10^{-2} \left(\frac{n_{\text{H}^+}}{10^{-2} \text{ cm}^{-3}} \right) \text{ M}_{\odot} \text{ yr}^{-1} \text{ kpc}^{-2}, \quad (5)$$

which should be closer to the Milky Way value for the same assumed densities.

6.2.2. Interface Models

Models in which the O VI ions occur in conductive interfaces or turbulent mixing layers (TMLs) make different predictions for the behavior of O VI column density with abundance. In the TML models, for example, the column density of O VI is related both to the specific properties of the mixing (e.g., the velocity shear and fraction of hotter material mixed into the turbulent layer) and the abundance of the oxygen in the material (Slavin et al. 1993). Therefore, in these models, the similarity in the Galactic and LMC values of N_{\perp} may simply be a coincidence dictated by the lower abundance of the latter modified by a greater amount of transition temperature material in the LMC compared with the Milky Way.

Increased amounts of gas in the O VI-producing temperature range may be related to different energy input into the ISM by massive stars (and their corresponding supernovae), or to differences in the interaction between hot and cool gas between the two galaxies (determined by unknown mechanisms which may include the metallicity or differences in the magnetic fields). If we assume that the physics of the mixing between the galaxies is similar, the increased quantities of hot gas in the interface models requires a higher energy input into the ISM in the LMC compared with the Milky Way.

A larger local energy input from massive stars in the LMC has some observational support. Tumlinson et al. (2001) have studied the excitation and photodissociation of H_2 in the LMC. Their models predict that the near-ultraviolet (NUV) flux per unit area of the LMC is a factor of ~ 10 higher than in the solar neighborhood of the Milky Way. If the NUV radiation field in the LMC is taken to be an indicator of the current density of massive stars, then this would argue for a correspondingly larger kinetic energy input into the ISM within the LMC through winds and supernovae.

Measures of the current star formation rate (SFR) and its surface density (which is more closely related to the energy input per unit area of the disk) also suggest the LMC should have a greater energy input into the ISM than the Milky Way. The SFR in the Milky Way is of order 2 to 5 $\text{M}_{\odot} \text{ yr}^{-1}$ (McKee & Williams 1997; McKee 1989; Mezger 1987), with average SFR per unit area of $\sim (2 - 8) \times 10^{-3} \text{ M}_{\odot} \text{ yr}^{-1} \text{ kpc}^{-2}$, depending on the adopted SFR and area over which the average is determined. For the LMC, the SFR is estimated to lie between 0.25 and 1 $\text{M}_{\odot} \text{ yr}^{-1}$ (Kennicutt et al. 1995 and Klein et al. 1989, respectively). The former measurement is derived from $\text{H}\alpha$ observations while the latter is from the thermal component of radio

continuum measurements. Given the probable effects of dust on the former, the higher value is somewhat preferred. Kim et al. (1998) determine that the bulk of the H I column of the LMC (which should correspond to the bulk of the star formation) occurs within a disk of diameter ~ 7.3 kpc. This implies a current SFR per unit area of $(6 - 24) \times 10^{-3} M_{\odot} \text{ yr}^{-1} \text{ kpc}^{-2}$ (with the higher value preferred). This also suggests a larger energy input per unit area in the LMC than in the local Milky Way, which would presumably lead to larger amounts of highly-ionized gas.

Distinguishing between the radiatively-cooling outflow and hot/cool gas interaction models as the origins of the observed O VI absorption will shed light on the structure and physics of a putative corona about the LMC and about the dependence of the feedback efficiency in galaxies on metallicity and stellar energy input. However, the current observations give little leverage for rejecting either class of models. The ratios of highly-ionized atoms in the gas can discriminate between pure radiatively cooling and TML-type models (see Spitzer 1996). Currently there are very few reliable observations of the other high-ion transitions (e.g., of C IV, Si IV, or N V) in the LMC. Bomans et al. (1996) have presented *HST* observations of C IV towards two stars projected within LMC 4, while Wakker et al. (1998) have presented *HST* observations of C IV absorption seen towards five stars within the “field.” None of these objects are included in the current sample of *FUSE* observations.

6.3. Kinematics of the LMC Corona

The kinematic profiles of Fe II and O VI along the sight lines in this work suggest that the O VI is kinematically decoupled from the thin interstellar disk of the LMC. The O VI is, on average, observed to be centered at velocities $\sim -30 \text{ km s}^{-1}$ from the Fe II centroids. There are two straightforward explanations for this kinematic offset of the O VI to more negative velocities: (1) rotation of a thickened disk or halo; and (2) outflow of highly-ionized material from the thin disk. Both of these explanations are compatible with our interpretation of the observed O VI properties of the LMC, i.e., that the O VI is indeed tracing a widely-distributed thick disk or halo of hot material.

A thickened disk of hot material that roughly rotates with the underlying thin interstellar disk of the LMC could produce the observed kinematic differences between the O VI and the Fe II. The ray from the Earth to a star in the disk of the LMC intersects the thin disk (traced by Fe II absorption) at essentially only the location of the star; however, because it is vertically-extended, the hot material (traced by O VI absorption) is sampled over a greater range of radial positions within the galaxy. Under the assumption of approximate corotation of disk and halo gas, this implies the O VI absorption will be observed over a greater range of velocities. In particular, assuming the H I velocity field (Kim et al. 1998) traces the rotation of the thin interstellar disk, the O VI is expected to occur at velocities generally lower than the Fe II in such a scenario. The maximum velocity of the O VI should be approximately equal to that expected of the thin disk at the position of the star, i.e., equal to the central velocity of the Fe II absorption. This is consistent with the velocity structure seen in Figure 9 (with a few exceptions).

A low-velocity outflow of highly-ionized material from the disk of the LMC could also explain the observed kinematic differences between the O VI and Fe II absorption profiles. If we assume that the outflow is purely perpendicular to the plane of the LMC, then the outflow velocity is $v_{\perp} \equiv \Delta v \sec i$, where Δv is the observed outflow velocity and i is the inclination of the LMC from the plane of the sky. Our observations then imply $\langle v_{\perp} \rangle \sim 40 \text{ km s}^{-1}$. The outflow of material from the disk is predicted in all models for the production of an interstellar galactic corona or thick disk. However, it is not clear whether one expects to

observe O VI associated with the outflow or the subsequent infall of material in various models. Models that produce O VI in radiatively cooling material require that the material ejected from the disk cool sufficiently from the very high temperatures at which the gas originates to temperatures where O VI is expected to be abundant. The observation of O VI in the outflowing material of a fountain flow would imply that the cooling time of the material was less than or of the order the sound crossing time of the halo (Houck & Bregman 1990). If the cooling time is sufficiently long (e.g., for low densities or very high initial temperatures), cooling through the temperatures at which O VI is abundant will not occur until the material ejected from the disk reaches its highest point and begins to infall.

For all of the sight lines probed by our observations there is O VI absorption at velocities that could imply the outflow of highly-ionized (O VI-bearing) gas from the thin disk of the LMC. However, in only two cases (towards Sk-68° 80 and Sk-70° 91) is there O VI absorption at velocities that might imply the infall of highly-ionized material. If a large-scale circulation of material through a corona about the LMC is occurring the majority of the gas must cool in the outflow phase of the circulation. We note that the velocities of the observed O VI absorption are low enough relative to the disk of the LMC that the material will not escape the galaxy altogether.

7. Summary

We have presented observations of 12 early-type stars within the Large Magellanic Cloud obtained with the *FUSE* observatory. These observations reveal strong absorption from interstellar O VI within the LMC. The main conclusions of our work are as follows.

1. Strong interstellar O VI at LMC velocities is present along all of the sight lines studied in this work. The observed stars probe a range of interstellar environments from stars within super-giant shells or superbubbles (e.g., Sk-71° 45, Sk-68° 80) to those in the field (e.g., Sk-67° 20, Sk-67° 05). A wide range of kinematic profiles for O VI within the LMC is also observed.
2. The column density of interstellar O VI at LMC velocities ranges from $\log N(\text{O VI}) = 13.9$ to 14.6 in atoms cm^{-2} , with a mean of $\log \langle N(\text{O VI}) \rangle = 14.37$ (with a dispersion of $\sim 40\%$). The average column density projected perpendicular to the disk of the LMC is $\log \langle N_{\perp}(\text{O VI}) \rangle = 14.29$, which is identical to the value derived from observations of the Milky Way halo even though the metallicity of the LMC is ~ 2.5 times lower than that of the Milky Way. The dispersions of the individual N_{\perp} measurements about the mean for each galaxy are also indistinguishable.
3. While our observations probe several sight lines projected onto superbubbles or other large-scale structures, any enhancements in the O VI column densities over those observed for field stars are minor ($\lesssim 50\% - 100\%$). The column density variations over the smallest scales probed by our observations ($\sim 450 - 510$ pc) are the same as those seen between sight lines towards and away from large-scale structures. Thus there is little evidence for enhanced O VI column densities towards superbubbles or other large-scale structures.
4. The average velocities of the LMC O VI absorption are different than those of the Fe II absorption, which traces low-ionization material associated with the disk of the LMC. The O VI velocities are on average shifted by $\sim -30 \text{ km s}^{-1}$ from the peak low-ionization absorption. This systematic displacement of the O VI to lower velocities may be the signature of a low-velocity outflow from the disk or of a rotating thickened disk.

5. Our measurements are not able to test for the existence of high negative velocity O VI in the LMC because of the overlap of Milky Way, IVC, HVC, and LMC absorption. The observations of all of the sight lines considered here are consistent with the presence of O VI outflowing from the LMC disk at relatively low velocities ($\lesssim 75 \text{ km s}^{-1}$). Material at positive velocities relative to the LMC disk, which could trace infalling material, is only allowed along the sight lines towards Sk-68° 80 and possibly Sk-70° 91. The former sight line shows gas which may be infalling at velocities $\sim 70 \text{ km s}^{-1}$ relative to the LMC disk.
6. The velocity dispersion of the O VI absorption is much greater than that of Fe II and other low-ionization species seen along the same lines of sight. The former is difficult to measure due to overlap between Milky Way and LMC absorption along many sight lines, but where measurable gives Gaussian dispersions of $\sigma \sim 30$ to 50 km s^{-1} . These breadths are much broader than the expected thermal broadening ($\sigma_{thermal} \sim 12 \text{ km s}^{-1}$ for $T \sim 3 \times 10^5 \text{ K}$), suggesting the presence of several absorbing components within the LMC O VI profiles.
7. We discuss the observed properties of interstellar LMC O VI in the context of a galactic “halo” or “corona” similar to that of the Milky Way. The striking similarity in the O VI columns and variations and in the observed velocity dispersions between the LMC absorption and that observed in the halo of the Milky Way motivate such a model. The observations are consistent with models of radiatively-cooling galactic fountain flows, although turbulent mixing layers and other types of interfaces are not ruled out. The radiatively-cooling fountain scenario is attractive since the predicted column density of O VI is not dependent on the metallicity of the cooling material.
8. If the O VI is produced in a galactic fountain flow, then the mass flow from one side of the disk of the LMC is estimated to be $\dot{M} \sim 1 M_{\odot} \text{ yr}^{-1}$, or alternatively, the mass flow rate per unit area of the disk is estimated to be $\dot{M}/\Omega \sim 2 \times 10^{-2} M_{\odot} \text{ yr}^{-1} \text{ kpc}^{-2}$. The cooling of this ejected material occurs before the gas begins to return to the disk. The average density of ionized hydrogen associated with the O VI-bearing gas likely exceeds $n_{\text{H}^+} \gtrsim 2 \times 10^{-4} \text{ cm}^{-3}$; studies of X-ray emission in the LMC suggest $n_{\text{H}^+} \sim 10^{-2} \text{ cm}^{-3}$, though this may sample denser gas than the O VI-bearing material. Better estimates of the physical state of the gas could be made with O VI emission line measurements towards the sight lines probed by our absorption line measurements.

We thank J. Gaustad and collaborators for the use of their H α image of the LMC. This image is from the Southern H-Alpha Sky Survey Atlas (SHASSA), which is supported by the National Science Foundation. We also thank Y.-H. Chu for help with the *ROSAT* X-ray mosaic. This work is based on data obtained for the Guaranteed Time Team by the NASA-CNES-CSA FUSE mission operated by the Johns Hopkins University. Financial support to U.S. participants has been provided by NASA contract NAS5-32985. JCH and KRS also recognize support from NASA Long Term Space Astrophysics grant NAG5-3485 through the Johns Hopkins University.

REFERENCES

- Bomans, D.J., de Boer, K.S., Koornneef, J., & Grebel, E.K. 1996, *A&A*, 313, 101
 Bregman, J.N. 1980, *ApJ*, 236, 577
 Brinks, E., & Bajaja, E. 1986, *A&A*, 169, 14

- Chu, Y.-H., Wakker, B.P., Mac Low, M.-M., & García-Segura, G. 1994, *ApJ*, 108, 1696
- Conti, P.S., Garmany, C.D., & Massey, P. 1986, *AJ*, 92, 48
- Crowther, P.A. & Smith, L.J. 1997, *A&A*, 320, 500
- Danforth, C.W., & Chu, Y.-H. 2000, *ApJ*, 552, L155
- Danforth, C.W., Howk, J.C., Fullerton, A.W., Blair, W.P., & Sembach, K.R. 2002, in preparation.
- Davies, R.D., Elliott, K.H., & Meaburn, J. 1976, *MmRAS*, 81, 89
- de Avillez, M.A. 2000, *MNRAS*, 315, 479
- de Boer, K.S., Braun, J.M., Vallenari, A., & Mebold, U. 1998, *A&A*, 329, 49
- de Boer, K.S., Koornneef, J., & Savage, B.D. 1980, *ApJ*, 236
- de Boer, K.S., & Savage, B.D. 1980, *ApJ*, 238, 86
- Deul, E.R., & den Hartog, R.H. 1990, *A&A*, 229, 362
- Dunne, B.C., Points, S.D., & Chu, Y.-H. 2001, *ApJS*, 136, 119
- Edgar, R.J., & Chevalier, R.A. 1986, *ApJ*, 310, L27
- Feitzinger, J.V., & Schmidt-Kaler, Th. 1982, *ApJ*, 257, 587
- Friedman, S.D., et al. 2000, *ApJ*, 538, L39
- Garmany, C.D., & Walborn, N.R. 1987, *PASP*, 99, 240
- Gaustad, J.E., McCullough, P.R., Rosing, W., & Van Buren, D. 2001, *PASP*, in press (see astro-ph/0108518)
- Gräfener, G., Hamann, W.-R., Hillier, D.J., & Koesterke, L. 1998, *A&A*, 329, 190
- Heiles, C. 1990, *ApJ*, 345, 483
- Henize, K.G. 1956, *ApJS*, 2, 315
- Holweger, H. 2001, in “Solar and Galactic Composition,” Ed. R.F. Wimmer-Schweingruber, in press (astro-ph/0107426)
- Houck, J.C., & Bregman, J.N. 1990, *ApJ*, 352, 506
- Jenkins, E.B. 1978, *ApJ*, 220, 107
- Kennicutt, R.C., Bresolin, F., Bomans, D.J., Bothun, G.D., & Thompson, I.B. 1995, *AJ*, 109, 594
- Kim, S., Dopita, M.A., Staveley-Smith, L., & Bessell, M.S. 1999, *AJ*, 118, 2797
- Kim, S., Staveley-Smith, L., Dopita, M.A., Freeman, K.C., Sault, R.J., Kesteven, M.J., & McConnell, D. 1998, *ApJ*, 503, 674
- Klein, U., Wielebinski, R., Haynes, R.F., & Malin, D.F. 1989, *A&A*, 211, 280
- Koesterke, L., Hamann, W.-R., Schmutz, W., & Wessolowski, U. 1992, *A&A*, 248, 166
- Kuntz, K.D., & Snowden, S.L. 2000, *ApJ*, 543, 195
- Lamers, H.J.G.L.M., & Cassinelli, J.P. 1999, *Introduction to Stellar Winds* (Cambridge: Cambridge Univ. Press)
- Lauroesch, J.T., Meyer, D.M., Sembach, K.R., Howk, J.C., & Welty, D.E. 2002, in preparation.
- Lehner, N., Fullerton, A.W., Sembach, K.R., Massa, D.L., & Jenkins, E.B. 2001, *ApJ*, 556, L103
- Leitherer, C. 1988, *ApJ*, 334, 626

- Mac Low, M.-M., & McCray, R. 1988, ApJ, 324, 776
- Massa, D., Prinja, R.K., & Fullerton, A.W. 1995, ApJ, 452, 842
- Massa, D., Fullerton, A.W., Sonneborn, G.S., & Hutchings, J. 2002, in preparation.
- McKee, C.F. 1989, ApJ, 345, 782
- McKee, C.F., & Williams, J.P. 1997, ApJ, 476, 144
- Mezger, P.G. 1987, in *Starbursts and Galaxy Evolution*, ed. T.X. Thuan, T. Montmerle, and J. Tran Thanh Van (Paris: Editions Frontières), p.3
- Moos, H.W., et al. 2000, ApJ, 538, L1
- Norman, C.A., & Ikeuchi, S. 1989, ApJ, 345, 372
- Oegerle, W.R., Murphy, E.M., & Kriss, G.A. 2000, The *FUSE* Data Handbook
- Oey, M.S. 1996, ApJ, 467, 666
- Patriarchi, P., & Perinotto, M. 1992, A&A, 258, 285
- Points, S.D., Chu, Y.-H., Snowden, S.L., & Smith, R.C. 2001, ApJS, 136, 99
- Press, W.H., Teukolsky, S.A., Vetterling, W.T., & Flannery, B.P. 1992, “Numerical Recipes in C: The Art of Scientific Computing,” (Cambridge: Cambridge University Press)
- Prinja, R.K., & Crowther, P.A. 1998, MNRAS, 300, 828
- Puche, D., Westpfahl, D., Brinks, E., & Roy, J.-R. 1992, AJ, 103, 1841
- Puls, J., Owocki, S.P., & Fullerton, A.W. 1993, A&A, 279, 457
- Russell, S.C., & Dopita, M.A. 1992, ApJ, 384, 508
- Sahnow, D., et al. 2000, ApJ, 538, L7
- Savage, B.D., et al. 2000, ApJ, 538, L27
- Savage, B.D., et al. 2002, in preparation.
- Savage, B.D., & de Boer, K.S. 1979, ApJ, 230, L77
- Savage, B.D., & de Boer, K.S. 1981, ApJ, 243, 460
- Savage, B.D., & Massa, D. 1987, ApJ, 314, 380
- Savage, B.D. & Sembach, K.R. 1991, ApJ, 379, 245
- Savage, B.D. & Sembach, K.R. 1994, ApJ, 434, 145
- Sembach, K.R. 1999, ASP Conf. Ser. 166, Stromlo Workshop on High-Velocity Clouds, ed. B.K. Gibson & M.E. Putman (San Francisco: ASP), 243
- Sembach, K.R., et al. 2000, ApJ, 538, L31
- Sembach, K.R., & Savage, B.D. 1992, ApJS, 83, 147
- Shapiro, P.R., & Benjamin, R.A. 1991, PASP, 103, 923
- Slavin, J.D., Shull, J.M., & Begelman, M.C. 1993, ApJ, 407, 83
- Smith, L.F., Shara, M.M., & Moffat, A.F.J. 1990, ApJ, 358, 229
- Smith, L.F., Shara, M.M., & Moffat, A.F.J. 1996, MNRAS, 281, 163
- Smith, R.C. 1999, in *New Views of the Magellanic Clouds, IAU Symp. #190*, ed. Y.-H. Chu, N. Suntzeff, J. Hesser, & D. Bohlender, p.28

- Snowden, S.L., & Petre, R. 1994, *ApJ*, 436, 123
- Spitzer, L. 1996, *ApJ*, 458, L29
- Tumlinson, J., et al. 2001, *ApJ*, submitted.
- Wakker, B.P., Howk, J.C., Chu, Y.-H., Bomans, D., & Points, S.D. 1998, *ApJ*, 499, L87
- Walborn, N.R. 1977, *ApJ*, 215, 53
- Walborn, N.R. 1982, *ApJ*, 254, L15
- Walborn, N.R., Lennon, D.J., Haser, S.M., Kudritzki, R.-P., & Voels, S.A. 1995, *PASP*, 107, 104
- Wang, Q., Hamilton, T., Helfand, D.J., & Wu, X. 1991, *ApJ*, 374, 475
- Welty, D.E., Frisch, P.C., Sonneborn, G., & York, D.G. 1999, *ApJ*, 512, 636
- Westerlund, B.E. 1997, *The Magellanic Clouds* (Cambridge: Cambridge Univ. Press)
- Yan, Z.-C., Tambasco, M., & Drake, G.W.F. 1998, *Phys. Rev. A*, 57, 1652

Table 1. Sightline and Stellar Properties for *FUSE* LMC Targets

Star	Alt. Name	α (J2000)	δ (J2000)	V [mag]	Sp. Type	Ref. ^a	v_∞ [km/s] ^b	Ref. ^c
Sk-67° 05 ^d	HD 268605	04 ^h 50 ^m 18 ^s .9	-67°39'38".2	11.34	O9.7 Ib	1	1665	1
Sk-67° 20	HD 32109	04 55 31.5	-67 30 01.0	13.87	WN4b	2	2900	2
Sk-66° 51	HD 33133	05 03 10.2	-66 40 54.0	12.69	WN8h	2	850	3
Sk-67° 69	...	05 14 20.2	-67 08 03.5	13.09	O4 III(f)	3	2600	4
Sk-68° 80	HD 36521	05 26 30.4	-68 50 26.6	12.40	WC4+OB	4
Sk-70° 91	LH 62-1	05 27 33.7	-70 36 48.3	12.78	O6.5 V	5	3000	5
Sk-66° 100	...	05 27 35.6	-66 55 15.0	13.26	O6 II(f)	6	2075	6
Sk-67° 144	HD 37026	05 30 12.2	-67 26 08.4	14.30	WC4	4	2600	7
Sk-71° 45	HD 269676	05 31 15.5	-71 04 08.9	11.47	O4-5 III(f)	1	2500	5
Sk-69° 191	HD 37680	05 34 19.4	-69 45 10.0	13.35	WC4	4	2800	7
Sk-67° 211	HD 269810	05 35 13.9	-67 33 27.0	12.26	O2 III(f*)	7	3750	8
Sk-66° 172	...	05 37 05.6	-66 21 35.7	13.13	O2 III(f*)+OB	7	3250	8

^aReference for the adopted spectral classification: (1) Walborn 1977; (2) Smith, Shara, & Moffat 1996; (3) Garmany & Walborn 1987; (4) Smith, Shara, & Moffat 1990; (5) Conti, Garmany, & Massey 1986; (6) Walborn et al. 1995; (7) Walborn et al. 2001.

^bStellar wind terminal velocity. The terminal velocities for the WR stars often have larger uncertainties than those for the O stars.

^cReference for the adopted wind terminal velocities: (1) Patriarchi & Perinotto 1992; (2) Koesterke et al. 1991; (3) Crowther & Smith 1997; (4) Leitherer 1988; (5) Massa et al. 2001; (6) Prinja & Crowther 1998; (7) Gräfener et al. 1998; (8) Walborn et al. 1995.

^dThe Sk-67° 05 data used here are from the early-release observations of Friedman et al. 2000.

Table 2. Log of *FUSE* Observations

Star	FUSE ID ^a	Start Date ^b	No. of Exp. ^c	Exp. Time [ksec]	S/N ($\lambda 1031$) ^d
Sk-67° 05	e	e	e	33.0	> 30
Sk-67° 20	P11744	10/12/2000	6	16.3	20
Sk-66° 51	P11745	09/30/2000	4	4.6	18
Sk-67° 69	P11717	12/20/1999	4	7.8	15
Sk-68° 80	P10314	12/17/1999	4	9.7	24
Sk-70° 91	P11725	10/05/2000	1	5.5	18
Sk-66° 100	P11723	12/20/1999	2	7.1	17
Sk-67° 144	P11750	02/12/2000	3	8.1	10
Sk-71° 45	P10315	10/02/2000	4	18.9	25
Sk-69° 191	P11751	02/12/2000	3	7.0	11
Sk-67° 211	P11716	12/20/1999	5	8.2	21
Sk-66° 172	P11722	09/26/2000	1	3.6	13

^aArchival rootname of target for FUSE PI team observations. All data were processed with versions 1.8.6 or 1.8.7 of the CALFUSE pipeline.

^bStart date of the observations. For the data presented here, the data were all collected within a few days of the first exposures.

^cNumber of individual exposures.

^dApproximate signal-to-noise ratio per 20 km s⁻¹ resolution element near the strong O VI transition at 1031.926 Å in the LiF1 channel.

^eThe observations of this star have been described by Friedman et al. 2000. These data required special processing since the star was stepped across the 30'' × 30'' LWRS aperture during the integrations. The data were acquired at various times between 08/20/1999 and 10/19/1999.

Table 3. Molecular Hydrogen Lines^a

λ [Å]	ID	$\log \lambda f$	Notes
$J = 3$			
1031.191	(6-0) P(3)	1.059	Contaminating line
1006.411	(8-0) R(3)	1.199	
1019.500	(7-0) P(3)	1.029	
1028.985	(6-0) R(3)	1.253	Blended: Ly β
1043.502	(5-0) P(3)	1.051	Blended: MW R(4)
1053.976	(4-0) R(3)	1.149	
1056.472	(4-0) P(3)	1.004	Blended: MW R(4)
1067.479	(3-0) R(3)	1.030	
$J = 4$			
1032.349	(6-0) R(4)	1.247	Contaminating line
999.268	(9-0) R(4)	1.219	
1023.434	(7-0) P(4)	1.031	
1035.181	(6-0) P(4)	1.067	
1044.542	(5-0) R(4)	1.209	Blended: LMC P(3)
1057.380	(4-0) R(4)	1.136	Blended: LMC P(3)
1060.581	(4-0) P(4)	1.017	

^aMolecular hydrogen lines used for determining contamination of interstellar O VI profiles. The (6-0) P(3) line at LMC velocities and (6-0) R(4) line at Milky Way (MW) velocities contaminate the O VI λ 1031.926 line when present. Lines marked as being blended refer to the LMC and Milky Way components for the $J = 3$ and 4 transitions, respectively. All of the listed lines are Lyman transitions.

Table 4. Equivalent Widths and Column Densities of Interstellar O VI in the LMC

ID	Star	W_λ [mÅ] ^a	$\log N(\text{O VI})^b$	v_-, v_+^c
1	Sk-67° 05 ^d	87 ± 5	$13.89^{+0.07}_{-0.06}$	+180, +325
2	Sk-67° 20	180 ± 10	$14.26^{+0.09}_{-0.10}$	+175, +335
3	Sk-66° 51	199 ± 21	$14.31^{+0.07}_{-0.07}$	+180, +365
4	Sk-67° 69	249 ± 11	$14.48^{+0.03}_{-0.03}$	+160, +345
5	Sk-68° 80	331 ± 7	$14.61^{+0.03}_{-0.04}$	+140, +330
6	Sk-70° 91	297 ± 9	$14.55^{+0.07}_{-0.08}$	+175, +375
7	Sk-66° 100	164 ± 15	$14.26^{+0.06}_{-0.05}$	+175, +315
8	Sk-67° 144	220 ± 16	$14.41^{+0.07}_{-0.06}$	+175, +335
9	Sk-71° 45	223 ± 5	$14.38^{+0.05}_{-0.06}$	+185, +350
10	Sk-69° 191	205 ± 18	$14.38^{+0.09}_{-0.10}$	+175, +330
11	Sk-67° 211	164 ± 6	$14.21^{+0.04}_{-0.04}$	+185, +375
12	Sk-66° 172	191 ± 14	$14.31^{+0.05}_{-0.06}$	+195, +365

^aEquivalent widths for the LMC material along the observed sight lines with 1σ error estimates. The error estimates include the effects of shifting the lower velocity integration limit by $\pm 20 \text{ km s}^{-1}$.

^bO VI column densities for LMC material along the observed sight lines with 1σ error estimates. In all cases these column densities have been derived using observations of the 1031.926 Å transition assuming no unresolved saturation is present. We adopt an f -value of $f = 0.1325$ from the theoretical calculations of Yan, Tambasco, & Drake 1998.

^cVelocity range over which the LMC profile was integrated.

^dThe O VI column densities towards Sk-67° 05 are taken from Table 2 of Friedman et al. 2000 assuming their “upper” continuum placement.

Table 5. Statistical Properties of Interstellar O VI in the LMC ^a

Quantity	Linear	Logarithmic
Full Sample		
Mean	2.34×10^{14}	14.37
Weighted Mean	1.80×10^{14}	14.25
Std. Deviation	$\pm 0.89 \times 10^{14}$	$+0.14$ -0.21
Median	2.37×10^{14}	14.38
New Observations ^b		
Mean	2.49×10^{14}	14.40
Weighted Mean	2.22×10^{14}	14.35
Std. Deviation	$\pm 0.78 \times 10^{14}$	$+0.12$ -0.16
Median	2.37×10^{14}	14.38

^aAll quantities quoted were derived from the linear column densities.

^bStatistics for the sight lines excluding that towards Sk-67° 05. This star, described in detail by Friedman et al. 2000, has continuum placement uncertainties that likely exceed those of the rest of our sample.

Table 6. Interstellar Environments of the Background Probes

ID ^a	Star	Nebulosity ^b	Description
1	Sk–67° 05	N3/DEM7	Diffuse, faint H II region
2	Sk–67° 20	...	Field star
3	Sk–66° 51	DEM56	Faint H II region
4	Sk–67° 69	DEM107	Faint H II region on periphery of KDSB GS 44
5	Sk–68° 80	N144/DEM199	Superbubble projected onto LMC 3
6	Sk–70° 91	N204/DEM208	Superbubble
7	Sk–66° 100	...	Interior of LMC 4
8	Sk–67° 144	...	Periphery of LMC 4
9	Sk–71° 45	N206/DEM221/KDSB GS70	Superbubble
10	Sk–69° 191	N154/DEM246/KDSB GS72	Superbubble
11	Sk–67° 211	N59A/DEM241	Bright H II region
12	Sk–66° 172	N64B/DEM252	Bright H II region on periphery of LMC 4

^aIdentifications corresponding to the labels in Figures 5, 6, and 7.

^bThe designations N and DEM refer to entries in the catalogs of Henize 1956 and Davies, Elliott, & Meaburn 1976, respectively. The designation KDSB GS refers to an entry in the Kim et al. 1999 catalog of “giant shells” identified in the Kim et al. 1998 H I mosaic of the LMC.

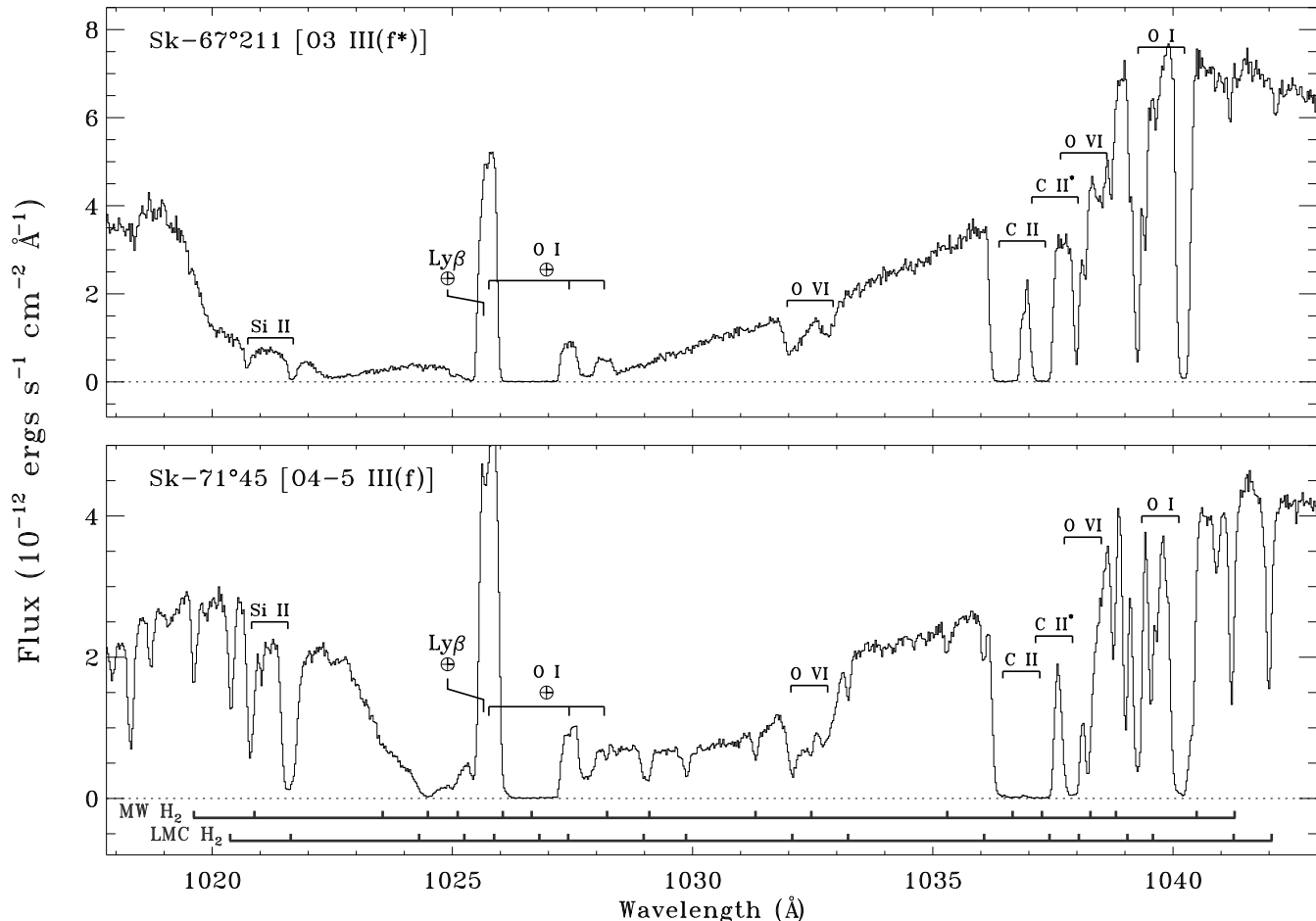


Fig. 1.— Sample *FUSE* spectra in the spectral region centered on 1030 \AA for the stars Sk-67° 211 (*top*) and Sk-71° 45 (*bottom*). The data shown in this figure have been rebinned to ≈ 27 m \AA , or ~ 7.8 km s^{-1} , per pixel for display purposes. Several ionic species seen in the ISM of both the Milky Way and LMC are marked, with the tick separation approximately corresponding to the velocity separation of the low-ion absorption along each sight line. Airglow lines are also indicated. The sight line towards Sk-71° 45 shows a rich H₂ spectrum in both the Milky Way and the LMC. The expected positions of H₂ transitions (for $J \leq 4$ only) are marked below this spectrum. The sight line towards Sk-67° 211 shows only very weak absorption from molecular hydrogen in both the Milky Way and LMC. The (6-0) P(3) and R(4) transitions of H₂ at rest wavelengths of 1031.19 and 1032.35 \AA , respectively, can contaminate the O VI λ 1031.926 absorption from the halo of the Milky Way.

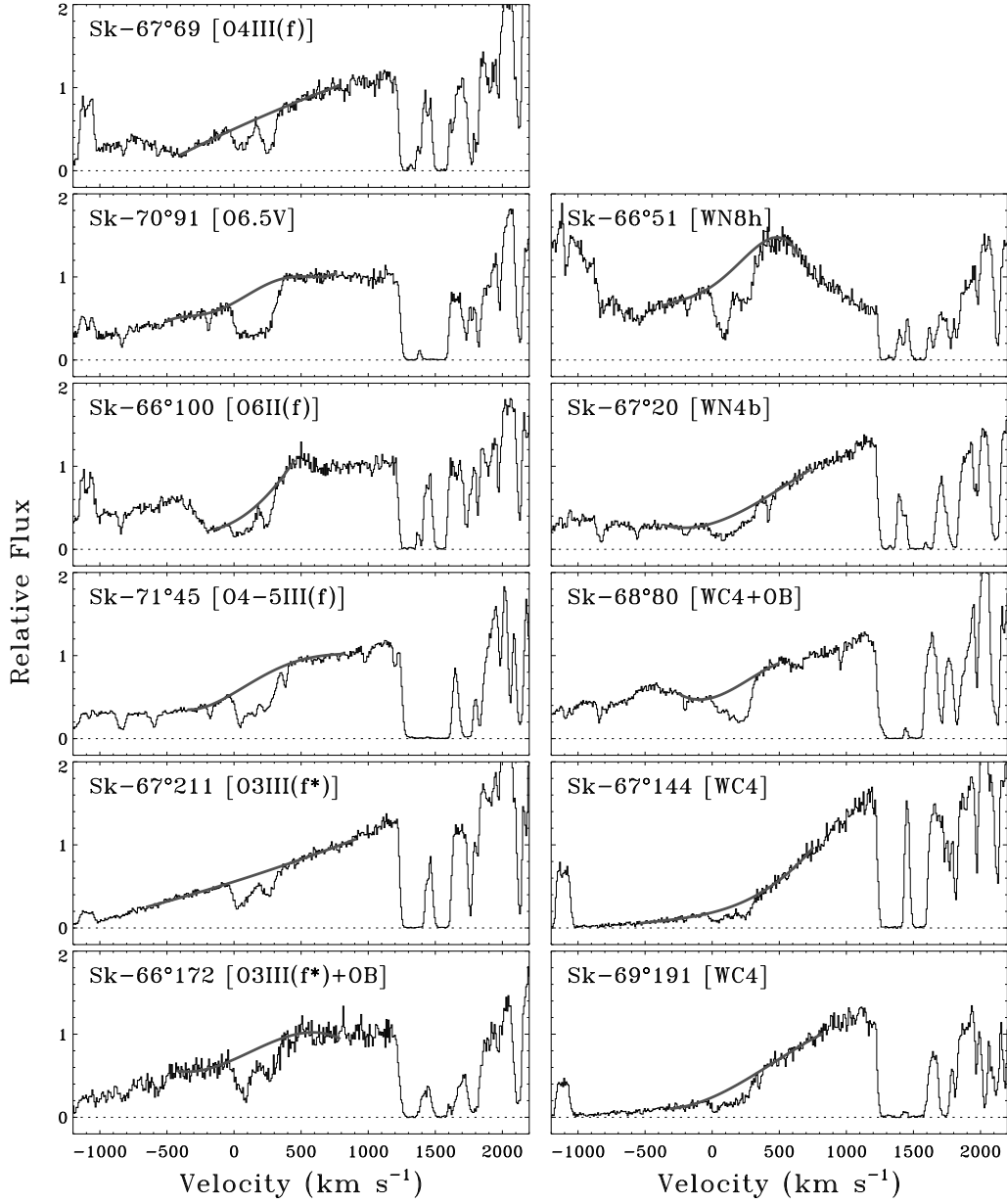


Fig. 2.— Sample fits to the stellar continua in the region of interstellar O VI $\lambda 1031.926$ absorption for the LMC O stars (*left*) and WR stars (*right*) studied in this work. The velocity scale is (approximately) relative to the LSR, and the data have been binned to ≈ 27 mÅ, or ~ 7.8 km s $^{-1}$, per pixel for display purposes.

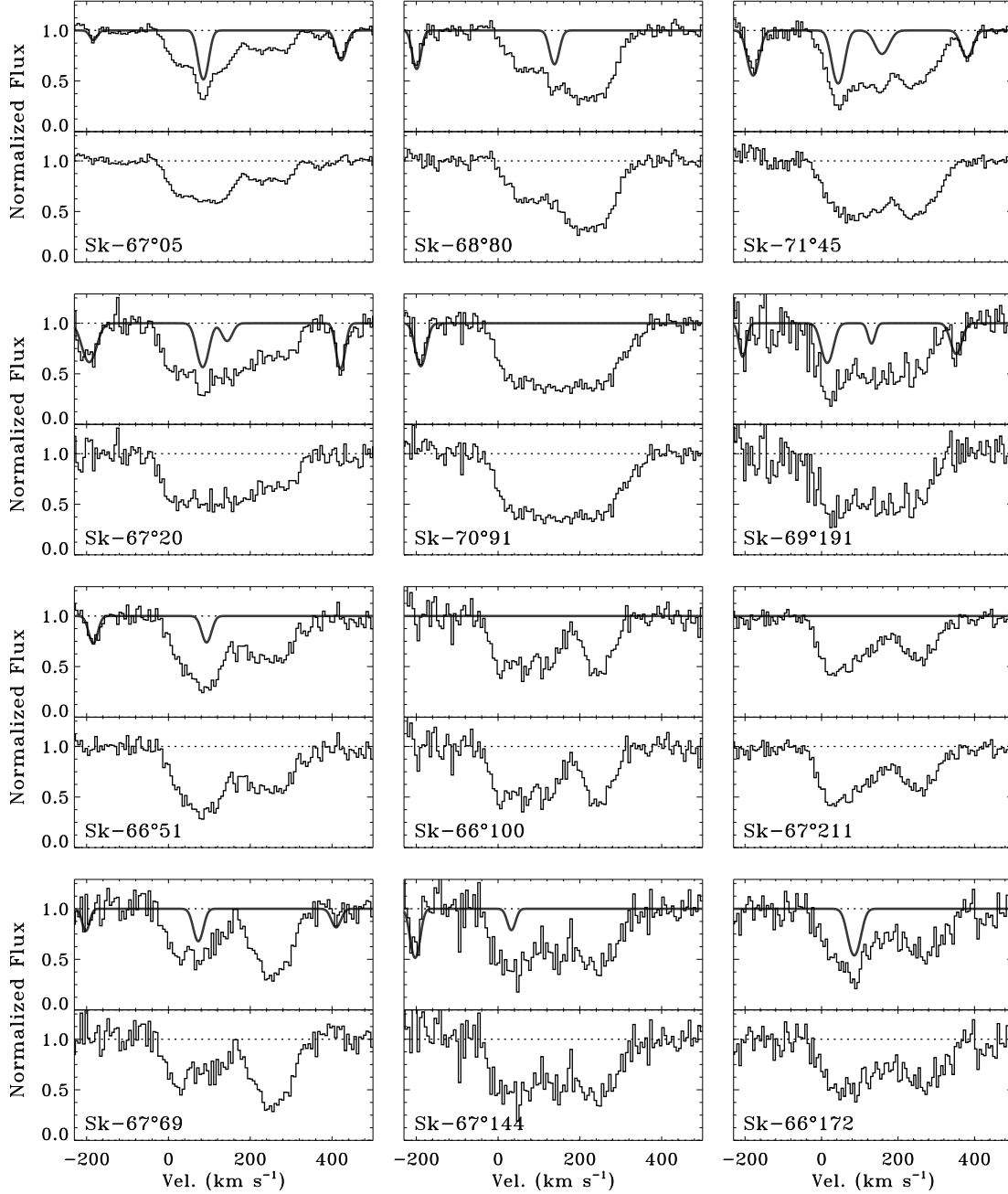


Fig. 3.— Continuum normalized interstellar O VI absorption profiles for the sight lines being considered in this work. For each star two panels are shown: the normalized O VI profiles with a model for the contaminating H₂ absorption overplotted (*top*) and the normalized profiles after division by the H₂ absorption model (*bottom*). These profiles are plotted after rebinning to 20 mÅ, or $\sim 6 \text{ km s}^{-1}$, per pixel.

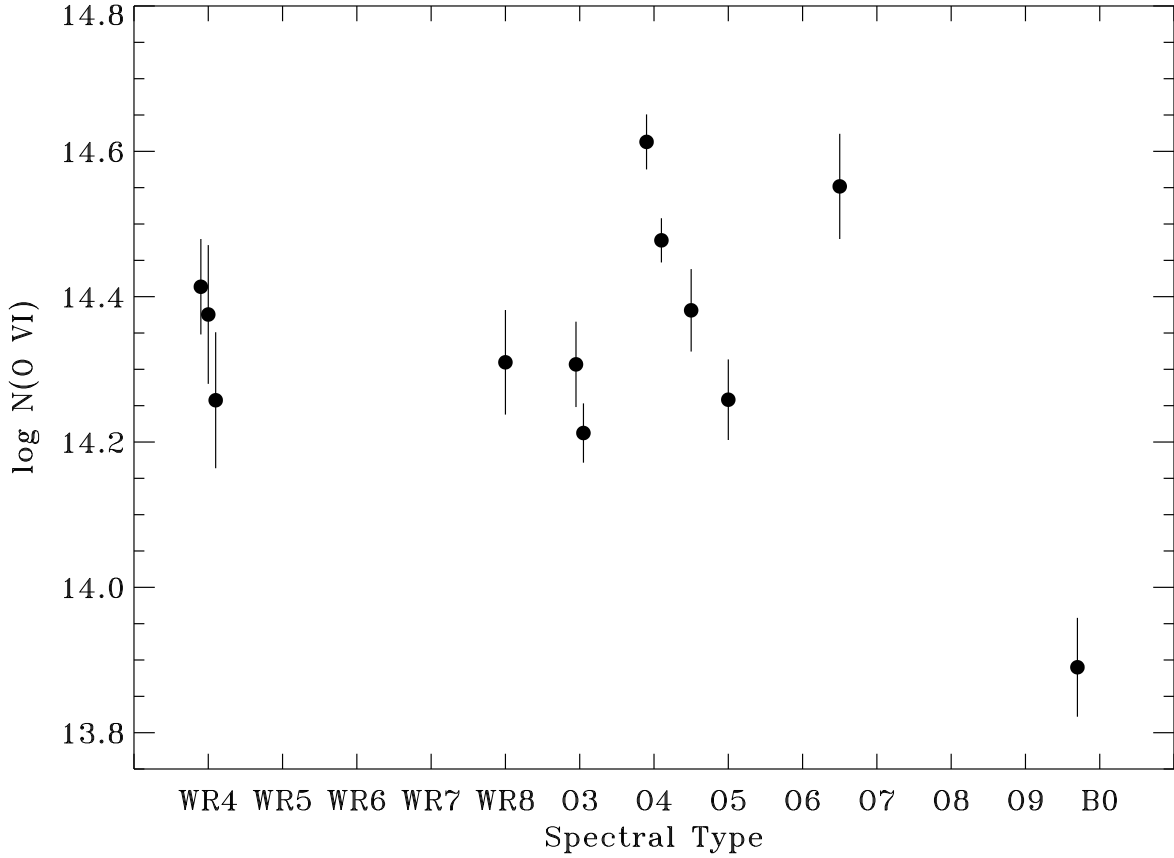


Fig. 4.— Interstellar O VI column in the LMC as a function of spectral type of the background probe. We see no apparent trends in the O VI column density with spectral type of the probe star, suggesting the local effects of the stars themselves may play a minor role if any in providing the observed O VI columns.

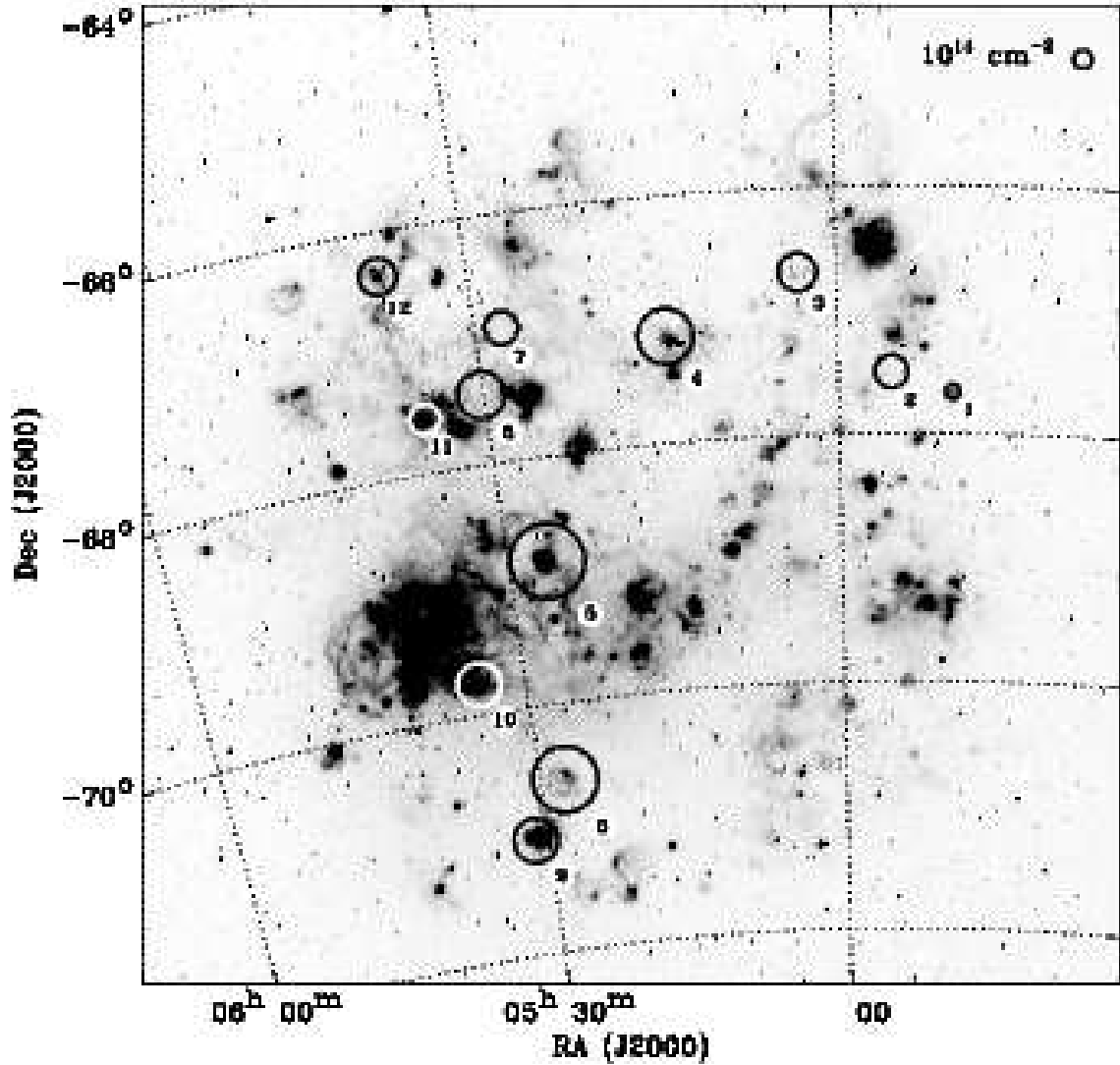


Fig. 5.— $H\alpha$ image of the LMC (Gaustad et al. 2001) with the positions of the probe stars marked. Darker regions correspond to brighter $H\alpha$ emission. The radius of the circle marking each probe star is linearly proportional to the column density of interstellar O VI at LMC velocities. For scale, a circle corresponding to $N(\text{O VI}) = 10^{14} \text{ cm}^{-2}$ is given in the upper right of the image. The numbers given beside each circle correspond to the identifications listed in Tables 4 and 6. Note that much of the apparent emission near Sk-67° 69 (#4) is caused by an imperfectly-subtracted foreground star.

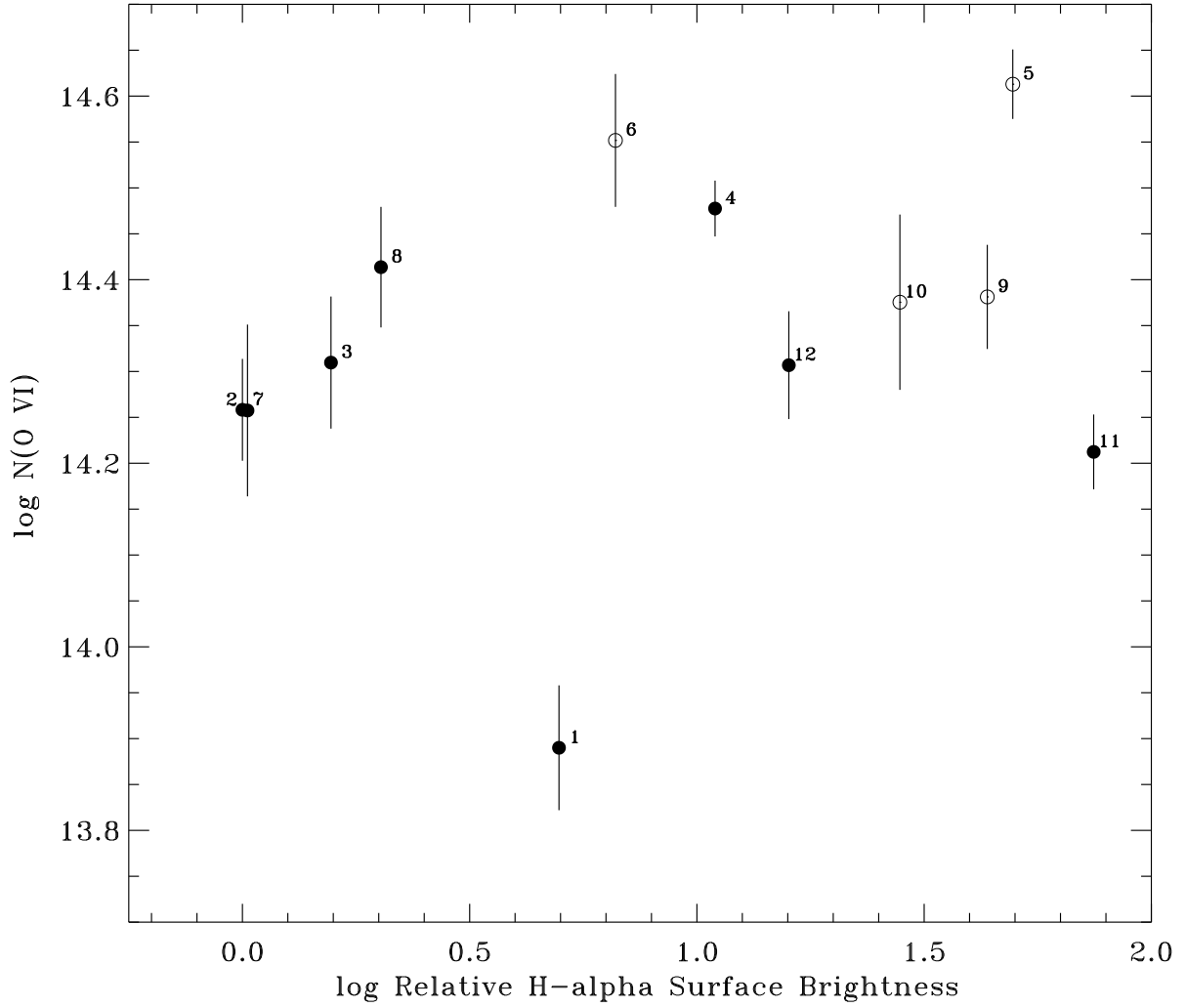


Fig. 6.— Interstellar O VI column density versus relative H α surface brightness (averaged over $6'6 \times 6'6 - 100 \times 100 \text{ pc}^2$ – boxes) for the sight lines studied in this work. The numbers given beside each point correspond to the identifications listed in Tables 4 and 6. Open circles denote directions towards identified superbubbles (see Table 6).

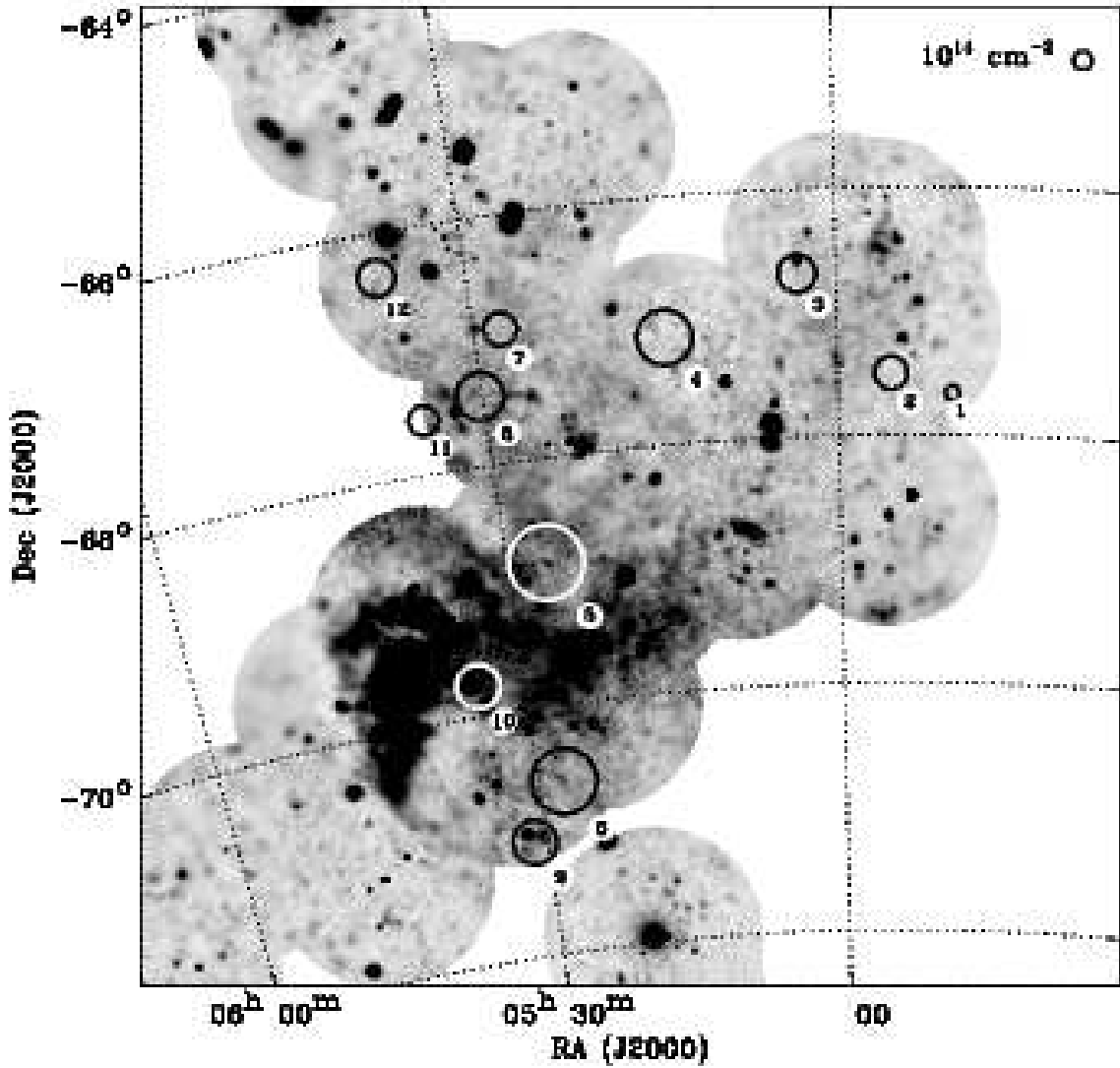


Fig. 7.— *ROSAT* PSPC mosaic of the LMC (Snowden & Petre 1994) with the positions of our probe stars marked. This image shows the R4–R7 band image, which covers the 0.5–2.0 keV energy range. The angular resolution varies with position in this adaptively-smoothed image, but is always larger than the $20''$ limit for the PSPC. Darker regions correspond to brighter X-ray emission. As in Figure 5, the radius of the circle marking the position of each probe star is linearly proportional to the column density of interstellar O VI at LMC velocities, with a scale given in the upper right. The numbers given beside each circle correspond to the identifications in Tables 4 and 6.

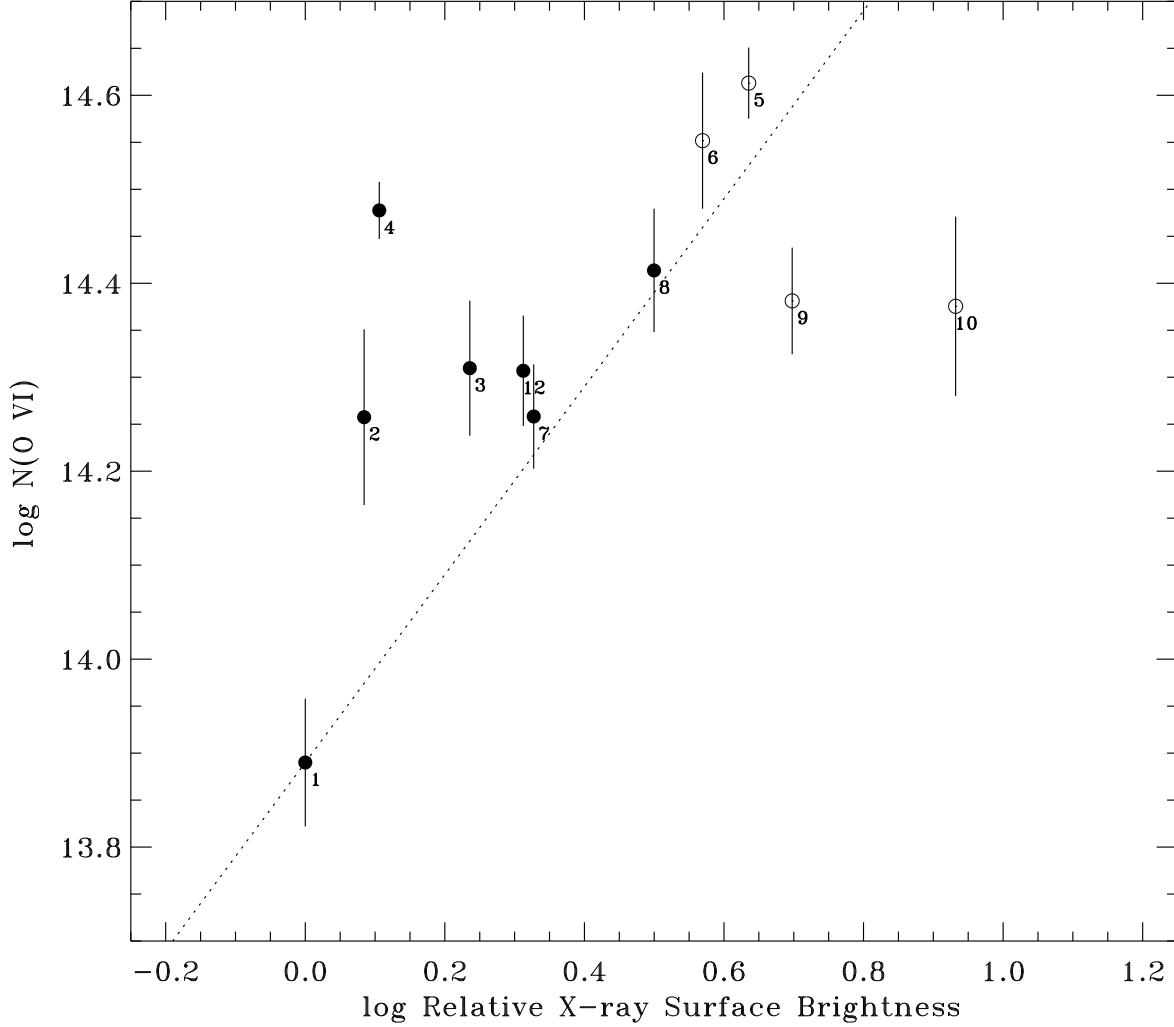


Fig. 8.— Interstellar O VI column density versus relative *ROSAT* 0.5 to 2.0 keV PSPC surface brightness (averaged over $6'6 \times 6'6 - 100 \times 100 \text{ pc}^2$ – boxes) for the sight lines studied in this work. The numbers given beside each point correspond to the identifications listed in Tables 4 and 6. Open circles denote directions towards identified superbubbles (see Table 6). The dashed line corresponds to a linear one-to-one relationship between the O VI column density and X-ray surface brightness. Note that the sight line towards Sk-67° 211 is not covered by the *ROSAT* mosaic and, therefore, is not represented in this figure. The lowest O VI column density is seen towards Sk-67° 05 (#1). The continuum placement for this star is less certain than for the other objects (see Friedman et al. 2000).

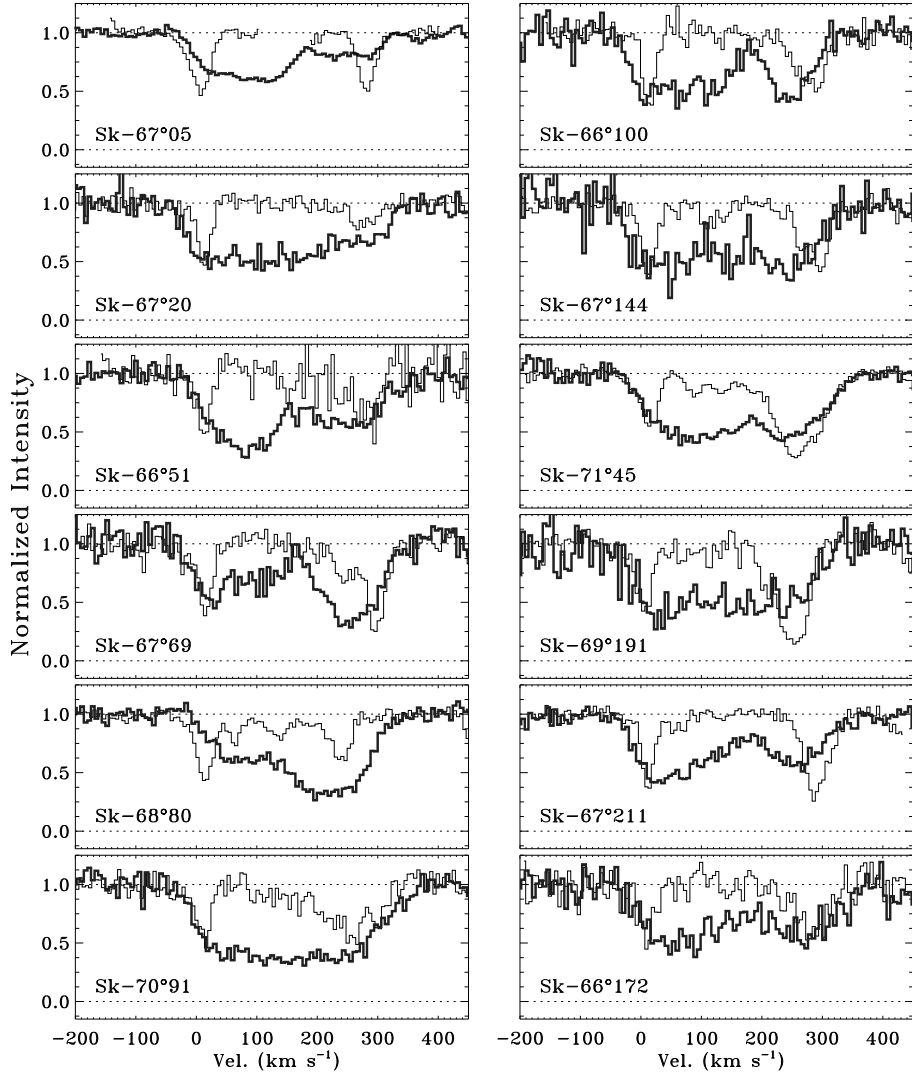


Fig. 9.— The observed absorption line profiles of O VI $\lambda 1031.926$ (thick line) and Fe II $\lambda 1125.448$ (thin line) towards the LMC stars studied in this work. The Fe II absorption components associated with the Milky Way and LMC are seen to be significantly narrower than the corresponding O VI profiles. Also present to some degree along all sight lines is gas associated with intermediate- and high-velocity clouds at $v \sim +65$ and $+125 \text{ km s}^{-1}$, respectively. The effective offsets of LMC O VI and Fe II absorption may be caused by rotational effects or by material outflowing from the disk. The Fe II profiles towards Sk-67°05 for velocities intermediate between the Milky Way and LMC absorption are not shown because of the presence of confusing stellar absorption at these velocities.